User Terminal Planar Antennas for Wireless Broadband Access at K_a Satellite Band

Filipe da Graça Gordo César de Faria

Thesis to obtain the Master of Science Degree in

Electrical and Computer Engineering

Supervisors:

Prof. Carlos António Cardoso Fernandes

Prof. Sérgio de Almeida Matos

Examination Committee

Chairperson: Prof. José Eduardo Charters Ribeiro da Cunha Sanguino

Supervisor: Prof. Carlos António Cardoso Fernandes,

Members of the Committee: Prof. Nuno Ricardo Cordeiro Leonor

January 2021

Declaração

Declaro que o presente documento é um trabalho original da minha autoria e que cumpre todos os requisitos do Código de Conduta e Boas Práticas da Universidade de Lisboa.

Declaration

I declare that this document is an original work of my own authorship and that it fulfils all the requirements of the Code of Conduct and Good Practices of the Universidade de Lisboa.

Acknowledgements

I would like to thank Instituto de Telecomunicações, UIDB/50008/2020, and project ADAM3D: PTDC/EEITEL/30323/2017, for financing all the needed material used in this thesis, and for the usage of IT laboratories, software, and hardware equipment.

I want to thank Mr. Carlos Brito and Mr. Farinha for all the help and availability in the construction process of the antennas.

I want to thank João Felício for all the help in assembling the prototype and for helping with CST STUDIO Suite.

I want to thank my supervisors Professor Carlos Fernandes and Professor Sérgio Matos for the guidance in these last months. For all the virtual meetings, insights and for always pointing in the right direction.

To Mestre Carlos Santos and Clube de Judo 2009, for keeping me active and being a place to push myself and relief my mind.

To all my friends and TUIST for all the good times. Thank you for all the memories and adventures we shared.

To Francisca, my best friend and my partner. Thank you for keeping me motivated through these long months. For always being there when I needed you.

To all my family, my mother, my father, and my sister for all the support. Thank you for keeping me company in this journey. Thank you for being there in all the successes and failures.

To all, my sincere thank you.

Abstract

Millimetre waves satellite communications systems are emerging as a viable solution to provide global broadband coverage. This endeavour poses several new challenges for the antenna design. Radial Line Slot Array (RLSA) antenna is a conventional leaky wave antenna that can be adapted to the new specifications of ground or space terminals, featuring high gain, low profile, and low cost.

This work presents a comprehensive study on the design of RLSA's, which requires an arrangement of a spiral like distribution of sub-wavelength slots in the upper plate of the circular parallel plate waveguide that compose the antenna. There is a wide variety of trade-offs to be considered in terms of the radiation and aperture efficiencies, bandwidth, cross-polarization, side lobe level and return losses. To have a systematic design method, two tools were developed: i) a GO/PO (Geometric Optics/ Physical Optics) framework for defining the antenna geometry; ii) a macro procedure that constructs the CAD (Computer Aided Design) model of the antenna for the full-wave analysis. Two antenna designs are presented in this work operating at 29.1 GHz: a RLSA that produces a boresight collimated beam with a 29.3 dBi gain; a second design that generates a 25.4º offset collimated beam with 26.4 dBi gain. Both designs have a diameter of 150 mm with only 1.61mm of height. A cavity-based feeding structure was also developed and optimized in order to simplify the manufacturing complexity of the RLSA antennas. Prototypes are being fabricated and measured, aiming to experimentally validate the promising full-wave results.

Keywords: leaky-wave antennas, satellite communications, CP-RLSA, beam-tilt, feeding cavity.

Resumo

Sistemas de comunicação por satélite de ondas milimétricas estão a emergir como uma solução viável para fornecer uma cobertura global de banda larga. Este esforço coloca novos desafios para a construção de antenas. Radial Line Slot Array (RLSA) é uma antena leaky-wave que pode ser adaptada às especificações dos terminais terrestres ou espaciais, apresentando alto ganho, baixo perfil e baixo custo.

Este trabalho apresenta um amplo estudo do processo de construção das RLSA, que requer uma disposição em espiral de slots na placa superior do guia de ondas. Os slots são dimensionados para que o seu comprimento seja menor que o comprimento de onda. Há uma grande variedade de compromissos a serem considerados em termos de eficiência de radiação e abertura, largura de banda, polarização cruzada, nível do lóbulos secundários e perdas por reflexões. Um método de desenho sistemático foi desenvolvido com duas ferramentas: i) uma estrutura GO/PO para definir a geometria da antena; ii) uma macro que constrói o modelo CAD para uma análise full-wave. Dois desenhos de antena são apresentados neste trabalho operando a 29.1 GHz: uma RLSA produz um feixe colimado vertical com um ganho de 29.3 dBi; outra RLSA gera um feixe colimado inclinado de 25.4º com um ganho de 26.4 dBi. Os desenhos têm um diâmetro de 150 mm com apenas 1.61 mm de altura. Foi também desenvolvida uma estrutura de alimentação baseada em cavidades, para simplificar a complexidade de fabrico das antenas. Os protótipos estão a ser fabricados para validar experimentalmente os resultados promissores.

Palavras-chave: antenas leaky-wave, comunicações via satélite, CP-RLSA, inclinação de feixe, cavidade de alimentação.

Contents

List of Figures

List of Tables

List of Acronyms

CAD – Computer Aided Design

CA-RLSA – Concentric Array RLSA

DBS – Direct Broadcast Satellite

DL-RLSA – Double-Layered Radial Line Slot Array

EM – Electromagnetic

GO/PO – Geometric Optics/Physical Optics

LEO – Low Earth Orbit

LHCP – Left-handed Circularly Polarized

MEO – Medium Earth Orbit

PEC – Perfect Electric Conductor

PMC – Perfect Magnetic Conductor

PPW – Parallel Plate Waveguide

RHCP – Right-handed Circularly Polarized

RLSA – Radial Line Slot Array

SLL – Side Lobe Level

SL-RLSA – Single-Layered Radial Line Slot Array

SOTM – Satcom On the Move

X-POL – Cross Polarization

Chapter 1

Introduction

1.1 Motivation and Objectives

In recent years, there has been an increase in the way information is accessed across the globe. There is a need for a reliable system which provides a high coverage area and a fast and strong connection. In response to this challenge, SOTM (Satcom On the Move) broadband access services with LEO (Low Earth Orbit) and MEO (Medium Earth Orbit) are being developed. A LEO satellite orbit altitude is near 2000 km or less and MEO satellites orbit from 2000 km to about 36000 km [1]. These satellites are linked in a network to form a web of satellites around the earth. These types of networks are commonly known as satellite constellations. Starlink by SpaceX is the most prominent system currently in development using this concept to provide worldwide internet cover [2]. There are 1015 LEO satellites in operation working in K_a (26.5 to 40 GHz) and K_u (12 to 18 GHz) frequency bands [3], [4]. It is expected the full network to reach at least 12000 satellites in total with future launches already scheduled [2].

For satellite access, the user must have an antenna to establish a connection. Typically, parabolic antennas or phase arrays are used for linking the user/base station with a satellite. Although they perform very well, the manufacture costs and high energy consumption for phased arrays and the large areas occupied by parabolic antennas are challenging. These two factors and the growing trend in the of satellite-based services require an alternative equivalent solution: a small, thin, light, and low-cost structure. This way a more widely available option can be produced.

Fig. 1 - Example of a Radial Line Slot Antenna [1]

The types of antennas explored in the MSc dissertation to meet these circumstances is a RLSA antenna. A RLSA is a circular structure comprised by two parallel plates and fed in the centre, normally by a coaxial cable, as represented in Fig. 1. The upper plate is filled with slots to allow radiation to escape. The slot positioning, length, width and angle orientation, antenna diameter and thickness affect

the manner in which the antenna functions. These parameters impact important aspects of antenna design.

A good beamwidth and a good beam shape are key to be able to send and receive a signal. It is required to have a pencil like shape with small side lobes to achieve good directivity, meaning the radiated energy will be directed at a precise direction. This energy must be radiated efficiently. This requires a good input impedance match and good radiation efficiency to achieve the required antenna gain value. Reflections inside the structure must be kept to a minimum to minimize its influence on the radiation pattern and to achieve the best possible bandwidth bandwidth.

Also, for this work a small antenna is preferred and thus a good precision is required during the manufacturing process. Certain dimensions are very small and, the slightest variance can greatly influence the final outcome of the work. Furthermore, a slim structure is more likely to be fragile so, the proper materials should possess structural sturdiness besides the intended electromagnetic properties. All this while striving for a low-cost approach.

1.2 State of the Art

In 1958, K. Kelly describes and experiments with a series of annular slot antennas. The experiment is successful in creating antenna prototypes with different radiation patterns and with linear or circular polarization. The working frequency of the antennas is 9 GHz. This is the first time the concept of RLSA is referred in literature [5]. K. Kelly and F. Goebels, in 1963, present new developments to the antenna although the antennas still present an intricate design. The antenna prototypes work with crossed slots and can operate using circular, linear, or elliptical polarization depending on the feed circuit. The theoretical analysis and experiments are carried in the X-Band (8 GHz - 12 GHz) [6].

In 1986, Ando et al. presented a design for a double-layered CP-RLSA (circular polarized RLSA). A practical theoretical foundation for the antenna design and equations are presented to place the slot pairs. These antennas work at 12 GHz [7][8]. Ando et al. successfully design a LP-RLSA (Linearly Polarized RLSA) in 1988. It is also used for satellite applications at 12 GHz. The slots are laid concentrically in pairs, with the same length, and are orthogonal and the antenna is double layered. These papers also describe a beam tilting technique to enhance the weak reflection coefficient which LP-RLSA tend to have [9], [10]. In 1992, Ando et al., publish a new technique to suppress internal reflection problems in LP-RLSA antennas: adding a reflection cancelling slot set. Antenna efficiency of 48% and 54% is measured for 40 and 60 cm diameter antennas, respectively, working at 12 GHz [11]. In 1990, Ando et al, propose a new SL-RLSA (single layered RLSA) at 12 GHz with circular polarization (CP-RLSA) by assigning a helicoidal geometric to the slots. A single layered RLSA requires a simpler fabrication process and a costs reduction overall. Two new techniques to improve antenna efficiency are also introduced: slot length and spacing variation and a matching spiral. In the first technique the slot lengths and their spacing may vary to synthesize a uniform aperture illumination. The latter is added to radiate the residual power at the edges of the antenna and reduce internal reflections to the feed. Antenna efficiency is 65% and the gain 34.5 dBi for a diameter of 60 cm [12], [13]. On the same year,

J. Hirokawa et al., develops a theoretical approach based on field equivalence theorem [14] to derive integral equations for the fields on the slots and the solution is then obtained using Galerkin's Method. For this method a CP-RLSA is considered at 12 GHz [15]. In 1991, M. Takashi et al., makes use of the techniques mentioned above to design single layered and small aperture CP-RLSA antennas at 12 GHz for Direct Broadcast Satellite (DBS) applications. To supress grating lobes the waveguide is filled with a dielectric material. The diameters are between 25 and 60 cm with an improved efficiency between 70 and 84%. For the 60 cm antenna the gain is 36.7 dB [16]. In 1992, the same authors, publish a more detailed account of the design process [17]. M. Ando publishes in 1993 an overview of the developments made in CP-RLSA applied in DBS (Direct Broadcast Satellite) reception. In the same year, J. Takada et al. prove the feasibility of having a SL-RLSA using a hollow waveguide. The gain presented is 33.5 dB Antenna efficiency is 61% with 50 cm of diameter and the antenna is working at 11.55 GHz [18]. In 1995, Takashi et al., introduce and apply beam tilting to a CP-RLSA by distributing the slot pairs over an elongated spiral. A 50 cm diameter antenna is designed with 67% efficiency and 33.7 dBi gain. The internal reflections show a good value [19].

In the 1990's, Davis and Bialkowski, two Australian researchers begin investigating RLSA antennas for DBS application. In 1997, Davis and Bialkowski, design a LP-RLSA antenna at the optimal frequency of 11.64 GHz with 35.6 dBi directivity of and 67% aperture efficiency. A set of reflection cancelling slots is used and disc-ended coaxial probe to feed the antenna [20]. In the same year, Davis et al., make the comparison between using beam tilting or reflection cancelling slots, in a LP-RLSA. The beam tilt used is 20º. Both significantly improve the return loss, with the beam tilting overperforming by little the reflection cancelling slots. The antenna gain is better when using the first technique for an operating frequency of 12.5 GHz [21]. In 1999, the same authors, test 55 cm LP-RLSA prototypes in the K_u band. A 20º beam squinted antenna and reflection cancelling slots are tested in comparison. Polypropylene is proposed as a low-cost material alternative to guide the waves inside the antennas [22]. In the same year, Davis et al., present a simple model to predict radiation patterns for both LP-RLSA and CP-RLSA. In the paper each slot pair is replaced by an equivalent magnetic dipole. Antennas at Ku- band with centre frequency at 12.5 GHz are considered. Theoretical values are in agreement with experimental values [23]. In 2000, Davis and Bialkowski, publish a review of the parameters and options of RLSA design such as polarization, antenna diameter, feed type, return loss improvement techniques, amongst others [24].

From 2000 onwards, researchers' efforts shift towards a computational solution by using modelling software, simulations, and algorithms to find an optimal design. In 2001, M. Sierra-Castañer et al., design several prototypes working at 12.1 GHz for TV-DBS application using measurements and comparisons based on MoM (Method of Moment) simulations previously developed by the authors. All the antennas are CP-RLSA [25]. In 2003, M. Vera-Isasa et al., publish a systematic design process for medium and high gain CP-RLSA antennas through the optimization of the slot pairs for good values of co-polar and cross-polar polarization values at 12.1 GHz [26] and a new design method for a beam tilted CP-RLSA [27]. For the latter, a good cross polarization ratio is achieved for an antenna working at 12.1 GHz with a 30.7 dBi directivity and a 10º tilt angle. In 2004, M. Ando, M Sierra-Castañer et al., design a CA-RLSA (concentric array RLSA) fed a rectangular waveguide feeder and analysed using the MoM.

The waveguide feeder has a cross slot transfer power to the upper circular waveguide. At 10 GHz, directivity is 21.8 dBi with 70% aperture efficiency for a 14 cm diameter antenna [28]. In the same year, M. Sierra-Castañer et al., apply the MSMM (Multiple Sweep Method of Moments) to improve a LP-RLSA. Image theory and free-space Green's function are used to calculate exterior and interior couplings between slots. The method is applied algorithmically allowing for slot position and length adjustments to compensate for phase shifts. A 47 cm diameter LP-RSLA antenna is presented with a 32 dBi gain [29]. In 2005, Sierra-Castañer et al., develop a fast method to analyse CP-RLSA [30]. The simulations with full-wave analysis are validated the results the authors get from 2 past experiments [31], [32]. In 2006, M. Albani et al., expand on the same idea of using a MoM formulation for a full-wave analysis to construct a CP-RLSA working at 18 GHz, 31 dBi of gain and 70.4% aperture efficiency [33]. In 2012, M. Albani et al., present a computational procedure to reduce higher spurious of electromagnetic (EM) wave modes from propagating and to perform beam shaping. Three models for CP-RLSA are designed based: pencil beam shape with controlled side lobe level (SLL), Isolux pattern, and pencil beam shape for maximum directivity pattern. All work at 22 GHz and present 80% total efficiency and good gain performance [34]. In 2014, the same authors, publish a design consisting in having 2 slot sets circularly polarized, one LHCP (Left-handed Circularly Polarized) and the other RHCP (Right-handed Circularly Polarized). The combined radiated waves result in a linearly polarized wave. A full-wave method of moments analysis proposed by the authors in [33] and [34] is used to optimize the design. The result has aperture efficiency of 49% and radiation efficiency of 98%. It works at 16.9 GHz [35]. In 2015, T. Nguyen et al., minimize the dielectric losses and enhance the antenna gain trough a new formulation for aperture slot coupling control in a 40 cm diameter CP-RLSA working at 60 GHz [36].

Due to the favourable dimensions of a RLSA antenna, literature also shows other applications besides satellite communications. Wi-Fi and point-to-point connections require small and reliable antennas. Purnamirza et al. have numerous papers referring the design and construction of RLSA applied to Wi-Fi [37]–[40].The bands used are 2.4 GHz and 5 GHz. It is also included the use of FR4: a low-cost and easy material to manufacture [41]. In 2012, the previous authors, introduce a new approach to beam tilting, calling it extreme beam squint technique. The paper proposes to increase the typical values beam tilting to increase reflection loss performance. The angles can be larger than 70^{o} with low gain values around 10 dBi [42].

More recently, new approaches continue to exist in the design of RLSA's. In 2019, Shao et al., present a dual-band design for RHCP at 12GHz and LHCP at 14GHz. The bands present a 18.02 dB gain with 40.18% aperture efficiency and 20.56 dB gain with 53.72% aperture efficiency, respectively [43]. In 2020, M. Lopez-Morales et al. present a combination of both a new analytic approach with optimization techniques based on current distribution, and energy conservation inside the antenna. The proposed design has gain of 35.6 dBi at 20 GHz [44]. Low-cost and all metal model for satellite communications is presented by N. Koli et al. A 36.3 dBi directivity antenna with a 56% aperture efficiency and 40 cm diameter is constructed [45].

1.3 Work Highlights

Two small aperture RLSA antenna are produced with a new type of feed: the first with a beam perpendicular to the antenna plane and the second with a beam tilt of 25.4º relative to the normal direction. The antennas have 150 mm in diameter and are very thin. The total height, including the feed, is around 4mm. The new proposed feed facilitates the assembly process by allowing precise adjustments of the coaxial cable inside the antenna. The structure works is in the K_a Band (26.5 – 40 GHz), with the best working frequencies ranging from 29.0 to 29.2 GHz. To reach all the previous features, a step-by-step analysis is made to ensure a good agreement between simulation and experimental results. For a pre-prototyping stage, a Wolfram Mathematica script called *KH3Dslot* [46] is used as a fast study method. Then, the model is designed using a CAD software to simulate EM (electromagnetic) wave propagation, *CST STUDIO SUITE*, and further modifications are made to boost antenna performance. The RLSA is fabricated using a printed circuit process. The top and bottom layers of the substrate are etched using photolithographic process. A proper fixture is designed and produced by 3D-printing to hold the antenna in the anechoic chamber for radiation pattern measurement.

This dissertation is divided into five chapters. The first chapter is an introduction of the dissertation's scope. It details the motivation and objectives of the work done and its main challenges. A literature review describing the solutions proposed by researchers in the field is also presented. The second chapter explains basic concepts and physical principles behind the working antenna and the methods and reasoning used for designing all the RLSA antenna parameters. Chapter three is the design and evaluation process of the model. It includes the computer simulation results and its subsequent analysis. Chapter four presents the manufacturing and performance results of the physical antenna model and compares it to previous simulations and other designs. The fifth and final chapter summarises the work by explaining the main achievements and suggesting future developments to the subject.

Chapter 2

Formulation and Methods

2.1 Basic Concepts and Physical Principles

2.1.1 Radial waveguides and propagation modes

Radial waveguides are a type of structure which supports the propagation of radial waves. An example of a radial waveguide are parallel plates. Two parallels placed at a distance *h* from each other and with EM source in the middle, as shown in Fig. 2 [47].

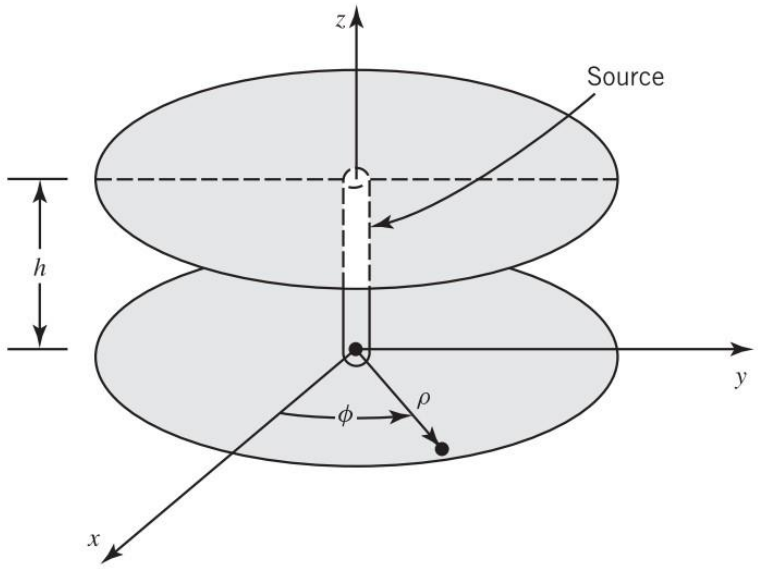

Fig. 2 – Radial waveguide: two parallel circular plates at h distance with a line source in the middle [47]

Radial waves travel in the radial direction ρ and equiphases are constant ρ planes. Radial waves variations in ρ direction are represented by first and second order Hankel Functions, $H_m^{(1)}(k_g\rho)$ and $H_m^{(2)}(k_g\rho)$, respectively. In this case Hankel Functions are used because they best describe the radial waveguide Transverse Electric (TE^z) and Transverse Magnetic (TM^z) Modes. Also known as Bessel functions of the third kind and represent a linear combination of Bessel function of first and second kind [47].

2.1.2 Babinet's Principle

Babinet's principle states: when the fields behind a screen with an opening is added to the field of a complementary structure, the sum is equal to the field when there is no screen [48]. For instances, this means field values for slotted antennas can be obtained by knowing the fields of its complementary form, various rectangles, or vice-versa. The principle can be exemplified as in Fig. 3.

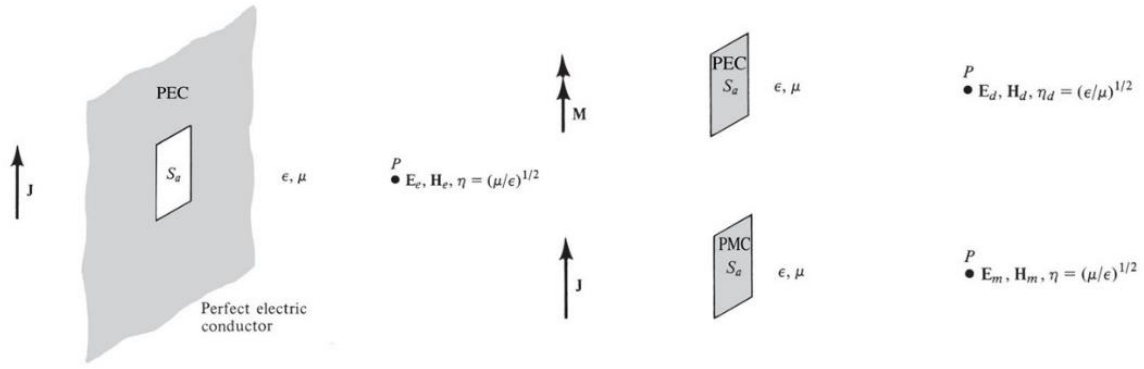

Fig. 3 – Babinet's Principle ilustration

On the left side of Fig. 3, a screen, PEC (Perfect Electric Conductor) in front of an electric radiating source **J**, has an opening S_a. The opening radiates to a medium with intrinsic impedance η and generates the fields, $\mathbf{E}_e$ and $\mathbf{H}_e$, at point P. The previous situation is equivalent to two different situations. In a medium with intrinsic impedance η_d a magnetic source **M** emitting in the presence of a PEC, S_a, produces at point P, the fields $\mathbf{E}_d$ and $\mathbf{H}_d$ or, in a medium with intrinsic impedance η an electric source **J** emitting in the presence of a PMC (Perfect Magnetic Conductor), S_a, produces at point P, the fields $\mathbf{E}_m$ and $\mathbf{H}_m$ [48]. From Babinet's principle, the latter obeys the following equations [48]:

$$\mathbf{E}_0 = \mathbf{E}_e + \mathbf{E}_m \tag{2.1}$$

$$\mathbf{H}_0 = \mathbf{H}_e + \mathbf{H}_m \tag{2.2}$$

$\mathbf{E}_0$ and $\mathbf{H}_0$ are the fields generate at point P by an electric source **J** with no opened screen or S_a, PEC or PMC. For the first equivalence the relation is as follows [48]:

$$\mathbf{E}_0 = \mathbf{E}_e + \mathbf{H}_d \tag{2.3}$$

$$\mathbf{H}_0 = \mathbf{H}_e - \mathbf{E}_d \tag{2.4}$$

2.2 RLSA – Radial Line Slot Array

Radial line slot array (RLSA) antennas are a form of leaky-waveguide antenna. They consist of a circular PPW (Parallel Plate Waveguide) which is fed at the centre to launch an outward travelling wave. The wave is then radiated by cutting slots cut on the top plate of the antenna. Slot dimensions and orientation will determine the type of wave synthesized. A rudimentary example of how it works is shown in Fig. 4. The structure is dependent on key elements which affect antenna performance and beam synthesis. This subsection lays out the necessary components and their dimensions to design the proposed antenna.

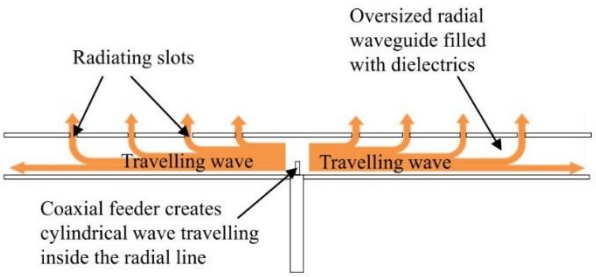

Fig. 4 – Example of how a RLSA works. [36]

2.2.1 PPW – Parallel Plate Waveguide

The waveguide is comprised of two circular parallel plates. An important feature to consider when designing the plates is the diameter. The larger the diameter, the longer a wave is propagated towards the edges. Thus, more power escapes trough the slots and less residual power remains inside the PPW. Also, the diameter should not be too small because antenna gain would be compromised and also cause return loss problems. Fig. 5 exemplifies the power flow present inside the structure. To set up the diameter, the frequency and application of the antenna must factor in the decision as it will impact the number and dimensions of the slots. An absorber is usually applied at the RLSA perimeter to lessen the effects of signal reflection into the feeder.

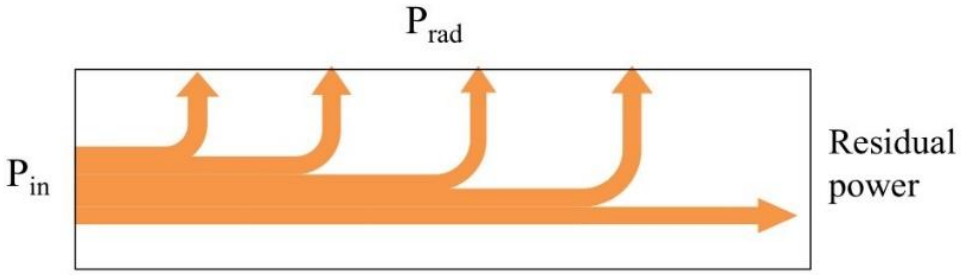

Fig. 5 – Power flow from antenna centre to edge. [36]

The height between the two plates is also a key aspect to take into consideration. To allow only the fundamental cylindrical mode $TM^{z}_{0,0}$ to propagate inside the waveguide the distance must obey the following condition [7]:

$$d < \frac{\lambda_g}{2}, \tag{2.5}$$

where, d represents the distance between the plates and λ_g represents the guided wavelength.

A dielectric substrate can be added between the plates to improve radiation pattern [17]. Array antennas are likely to produce secondary lobes as big as the main lobe. By spacing the array elements accordingly, in this case the slot pairs on the top plate, the in-phase addition of radiated fields in more than one direction is reduced. These unwanted lobes are called grating lobes [48]. The guided wavelength is given the equation [48]:

$$\lambda_g = \frac{\lambda_0}{\sqrt{\epsilon_r}}, \tag{2.6}$$

where, λ_0 represents the free-space wavelength and ε_r the dielectric material relative electric permittivity.

2.2.2 Slot Pair for Circular Polarization

The slots are arranged in a particular manner to achieve circular polarisation. There are three conditions to accomplish such polarisation. First, the field is required to have two orthogonal linear components, meaning that the field components have a 90º difference in space. Second, those two components must have the same magnitude. And finally, the field components must have a time-phase difference of odd multiples of $\frac{\pi}{2}$ radians, which is equivalent to delaying one of the components by the referred sum. These three conditions are necessary and sufficient to create circular polarization [48]. Fig. 6 illustrates the conditions explained previously by showing the field vector components and the resulting field.

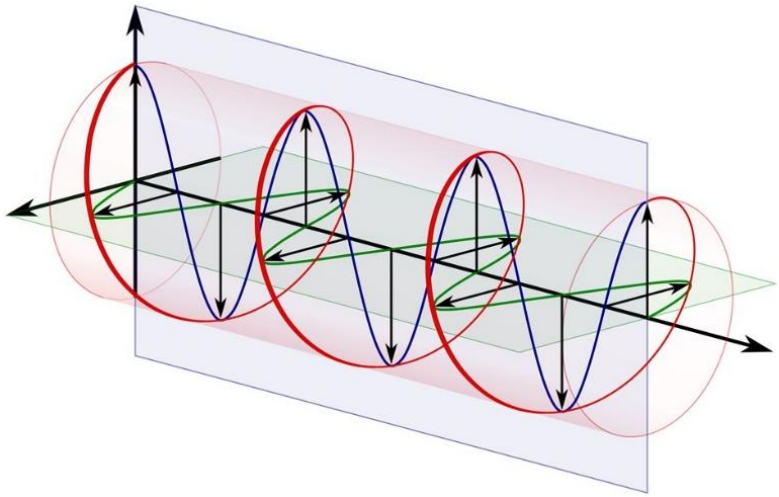

Fig. 6 – Circular polarized wave: blue and green field represent orthogonal fields with a phase shift and red represents the resulting field trace as a function of time [49].

A slot pair must be designed to implement these conditions. Each unit of the array contains a pair of slots that are placed orthogonally. This translates to a 90º angle between the two slots and 45º angle between the first slot and the radial direction. The orthogonal placement is responsible for generating two orthogonal electric fields. If the slots are placed as shown in Fig. 7, RHCP is achieved. If they each individual slot in Fig. 7 is rotated by 90º then, LHCP is achieved. Next, to produce the same field magnitude, the slots are equal in size. Both length and width are kept the same in a slot pair. Lastly, to secure a phase difference of $\frac{\pi}{2}$ radians between both generated fields, the following condition is applied based on Hankel functions [7]:

$$\arg\left(H_1^{(1)}(k_g\rho_2) \right) - \arg\left(H_1^{(1)}(k_g\rho_1) \right) = \frac{\pi}{2} \tag{2.7}$$

By simplifying the previous criteria, the two slots are separated by a quarter of λ_g. Thus, to establish the distance between slots the following expression is used as in reference [45]:

$$\rho_2 - \rho_1 = \frac{\lambda_g}{4}, \tag{2.8}$$

where ρ_1 and ρ_2 are the positions of both slot centres in relation to the centre, respectively, as depicted in Fig. 7.

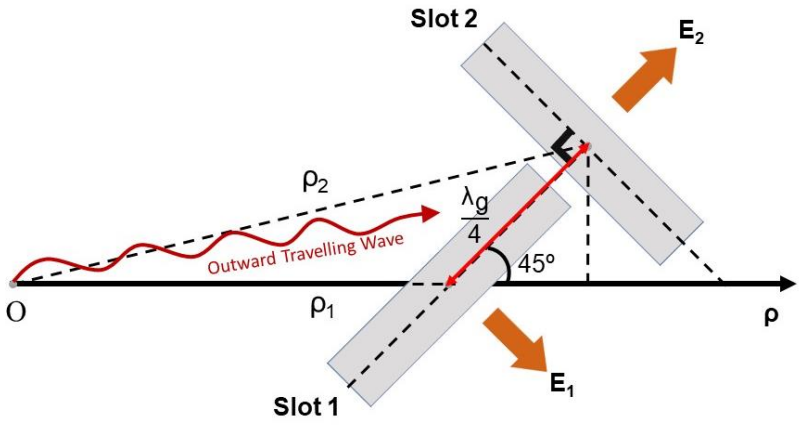

Fig. 7 – Slot Pair RHCP key features to generate orthogonal fields with a time-phase difference of $\frac{\pi}{2}$ radians

2.2.3 Aperture distribution

Each slot acts as a half-wavelength dipole, as described by Babinets' Principle [48] and is excited by outward travelling cylindrical wave. Slots are placed to couple with the currents on the top plate, so the magnetic field inside the waveguide determines the radiated fields [7]. The fields inside the PPW are given by an asymptotic approximation of the Hankel Functions. When $k_g\rho >> 1$, the following describes the magnetic field inside [7]:

$$H_\varphi = H_1^{(1)}(k_g\rho) \approx \sqrt{\frac{2}{\pi\, k_g\rho}}\, e^{-j(k_g\rho - \frac{3\pi}{4})}, \tag{2.9}$$

Where ρ is the radial coordinate and k_g is the guided wave number. The slots are placed in helicoidal shape. The contributions of all the individual slot pairs accomplish a directive beam. However, when making the spiral arrangement, slot pairs need to keep their relative angle with respect to radial direction for all the rotations. This means every azimuthal rotation is responsible for adding a phase factor $e^{-j\varphi}$ the slot placement must compensate so that all the radiating slots are fed in phase [7]. If the slot arrangement is not helicoidal but rather concentric, where several slot rings are set around the centre of the antenna, the approach would be different. All the slot pairs in each ring would be at the same distance from the middle, thus radiating in phase and not in need of compensating for the phase difference.

For an helicoidal distribution, slot pair density over top plate is defined as: $S_\varphi \times S_\rho$. S_φ is the

azimuthal distance between adjacent slot pairs and S_ρ is the radial spacing between slot pairs [7]. S_φ is defined arbitrarily, and various values are considered throughout the work. The phase factor compensation mentioned before is responsible for making S_ρ value defined as a guided wavelength, λ_g. Fig. 8 illustrates the described distances between the pairs in the slot spiral.

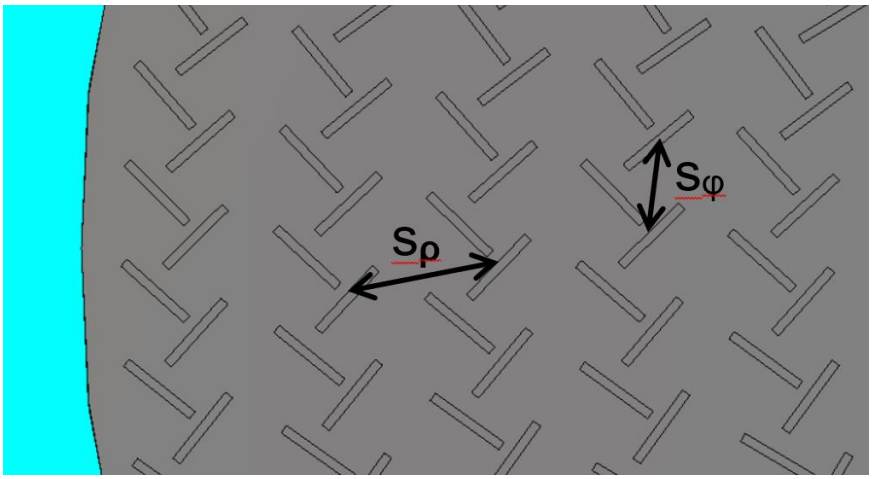

Fig. 8 - Slot Density: Sφ is the azimuthal distance and Sρ is the radial spacing.

For placing each pair accordingly, [7] presents the basis for every RLSA designing work. Fig. 9 represents all the key parameters for a slot pair. θ_1 and θ_2 are the inclination angles with the radial direction, **ρ**. W is slot width and L slot length. The width is kept constant while the length may vary, or it can remain constant. If the length remains constant, for DL-RLSA, its value is half of the guided wavelength, $\lambda_g/2$. The length can be varied with the radial direction **ρ**, to achieve good energy slot coupling and a uniform field distribution [13].

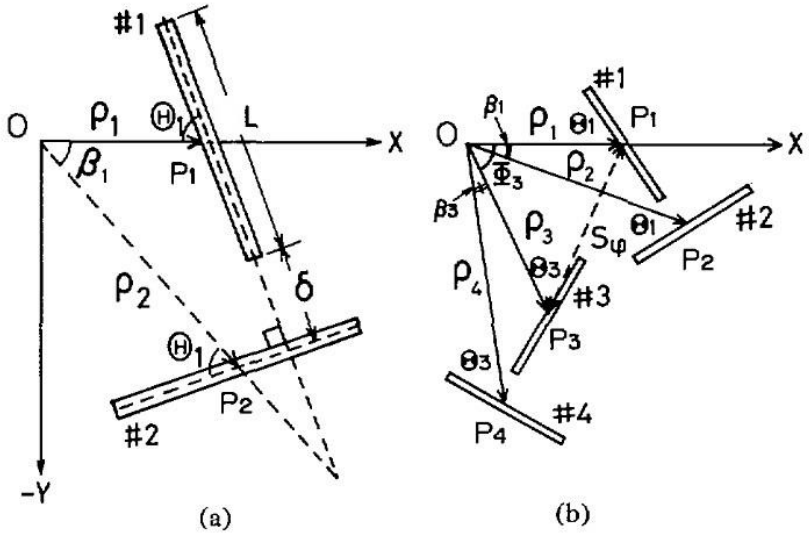

Fig. 9 – A slot pair of a CP-RLSA layout process described in [7]

Various expressions are used to compute the slots' positions and orientation. According to [7], the value of the first slot of the first pair must be set by applying the expression given by (2.7), the radial distances, ρ_1 and ρ_2, are determined. Then the following equation is used [7]:

$$\rho_2 \sin\Theta_1 - \rho_1 \cos\Theta_1 = \frac{L}{2} + \delta, \tag{2.10}$$

Θ_1 represents the angle each slot has with the radial line, and δ the distance between slots. Once the orientation Θ_1 is attained [7]:

$$\beta_1 = 2\Theta_1 - \frac{\pi}{2}, \tag{2.11}$$

where β_1 is the same slot pair angular distance. After concluding the first pair unit, the parameters for the next one is calculated. Φ_3 and ρ_3 express the value of the pair. Φ_3 is the rotation value from the first slot of the previous pair and the first slot of the pair, while ρ_3 is the radial distance of the first slot of the next pair. Their values are obtained by [7]:

$$\Phi_3 = \arg(H_1^{(1)}(k_g\rho_3)) - \arg(H_1^{(1)}(k_g\rho_1)), \tag{2.12}$$

$$S_\varphi{}^2 = \rho_1{}^2 + \rho_3{}^2 - 2\rho_1\rho_3 \cos\left\{ \arg(H_1^{(1)}(k_g\rho_3)) - \arg(H_1^{(1)}(k_g\rho_1)) \right\} \tag{2.13}$$

If the condition $k_g\rho >> 1$ is true, equation (2.12) can be simplified according to [7]:

$$\rho(\theta) = \rho_0 + \theta\frac{\lambda_g}{2\pi} \tag{2.14}$$

The previous equation indicates radial distance, $S\rho$, between each spiral turn will be λ_g. All the features slot design and placement are shown in Fig. 9.

For this work, an expansion on the previous equation is used to obtain the angle of rotation for each slot pair for an arbitrary arc length. Multiplying both sides of (2.14) results in an elementary arc length $d\ell$, according to:

$$\rho\, d\theta = \rho_0 d\theta + \theta\frac{\lambda_g}{2\pi} d\theta = dl \tag{2.15}$$

For an arbitrary angular interval between θ_1 and θ_2, the corresponding arc length is calculated by performing the following line integral:

$$arclen = \int_{\theta_1}^{\theta_2} \rho_0 d\theta + \frac{\lambda_g}{2\pi}\int_{\theta_1}^{\theta_2} \theta\, d\theta \tag{2.16}$$

This integral has a closed-form solution:

$$arclen = \rho_0(\theta_2 - \theta_1) + \frac{1}{k_g}\left[\frac{\theta^2}{2}\right]_{\theta_1}^{\theta_2}, \tag{2.17}$$

$$arclen = \rho_0(\theta_2 - \theta_1) + \frac{1}{2k_g}(\theta_2{}^2 - \theta_1{}^2), \tag{2.18}$$

$$2k_g arclen = 2k_g\rho_0(\theta_2 - \theta_1) + \theta_2{}^2 - \theta_1{}^2 \tag{2.19}$$

and

$$\theta_2{}^2 + 2k_g\rho_0\theta_2 - (2\, k_g arclen + 2k_g\rho_0\theta_1 + \theta_1{}^2) = 0 \tag{2.20}$$

Now we solve for θ_2 using a simple quadratic formula and get:

$$\theta_2(\theta_1) = - k_g\rho_0 + \sqrt{(k_g\rho_0)^2 + 2k_g arclen + 2k_g\rho_0\theta_1 + \theta_1^2}, \quad (2.21)$$

where *arclen* represents the azimuthal distance between two radiating slot pairs, S_φ, which will be kept constant between consecutive slots in the spiral path. To control the azimuthal distance between slot pairs, an arbitrary constant *r* is assigned, and the distance is correlated to the guided wavelength. The subsequent equation represents said control:

$$arclen = r \cdot \lambda_g \quad (2.22)$$

2.2.4 Feeding Structure

The feed is responsible for suppling energy to the antenna. There are two main approaches when feeding a RLSA antenna. In a single-layered RLSA, the simplest approach is to insert the coaxial cable antenna centre and making direct contact with the dielectric material inside and adjustments need to be made to determine the best transfer of power [45]. For example, the depth of insertion inside the waveguide and what kind of termination the cable will have. The cable's end can remain simple or need a termination. For instance, a disk or a cone like shape can be added as in Fig. 10.

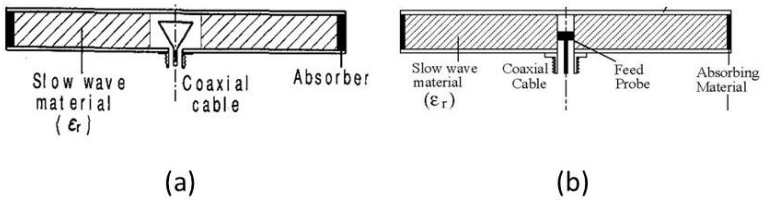

Fig. 10 – Single Layer RLSA Feeds: coaxial cable is terminated by a cone (a) [11] or a disk (b) [24].

When a RLSA antenna is double layered, the feeding process is made by the inserting the cable in the lower layer. The wave travels towards the edges and then bends into the upper layer where the energy will be radiated as illustrated in Fig. 11.

Another element to factor in both cases, are the cables' specifications. The power is fed through a coaxial cable which can vary in diameter and material. Usually, the cables have a copper core with a Teflon dielectric shielding. The model must be chosen accordingly. Also, an absorbing material can be placed to lessen the impact internal reflections thus improving the feeding process.

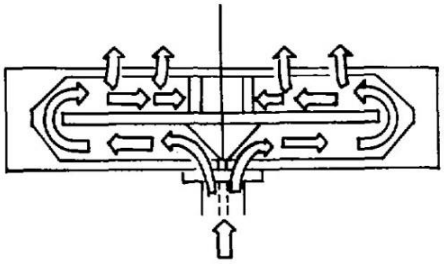

Fig. 11 – Double Layer RLSA Feeding Structure [7].

During this work, the initial approach regarding a feeding structure is similar to the one described for single-layered RLSA. The construction complexity and height of a DL-RLSA, makes it undesirable to pursue such configuration. A SL-RLSA simplifies the structure complexity by reducing the antenna to only one layer. The antenna can reach small dimensions. It can reach thickness of 2 mm approximately and it becomes difficult to tweak with precision the cable position inside the antenna. Due to such manufacturing constraints, a hybrid version is proposed to establish an accessible and simple construction process.

This hybrid feed consists of opening a circular aperture on the bottom plate of the PPW and then connecting it to small opened-ended cavity. Naturally, the proposed cavity is cylindrical and coaxial with the antennas' centre to produce an outward travelling wave, just as the previous examples.

To achieve a good coupling between the feed and the upper waveguide, a similar approach to the PPW height is considered. To avoid higher modes from propagating inside the feed, the height follows the condition described in equation (3.1). Thus, making sure the feeding wave only propagates in the fundamental mode $TM^{z}_{0,0}$. Also, by knowing the feeding structure is filled with air, free-space propagation is considered. Two other parameters need to be defined: the cavity diameter and the coaxial cable penetration depth inside the cavity. The range of tested diameter values is limited by the position of the first slots. On the other side, the penetration of the coaxial bale is limited by the height of the cavity. The more exposed the cable is inside the cavity, the more vulnerable to reflection problems it will become. On the other hand, the less cable is present inside, the antenna can become more susceptible to less power being fed. Therefore, a good trade-off must be achieved.

The feed and its features are as shown in Fig. 12. The height of the cavity and the cables' height inside the feed are represented by h_{cavity} and $h_{cable,}$ respectively. The opening diameter at the bottom of the feed is dependent of cable, and its diameter is d_{in}. Finally, the feed's radius is given by r_{cavity}.

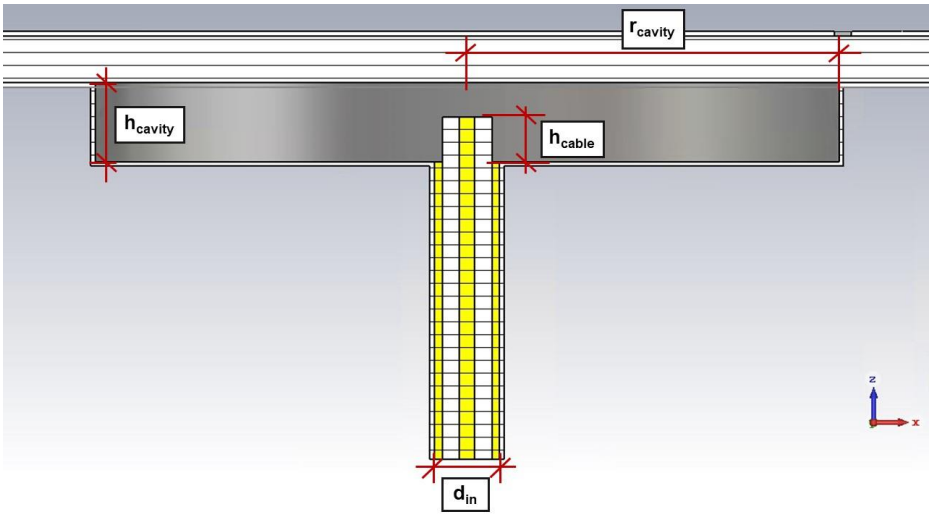

Fig. 12 – RLSA Feeding solution proposed. The dimensions are represented by the following variables: h_{cavity} – height of the cavity, h_{cable} – height of then cable inside the feed, d_{in} – diameter of the opening for cable insertion and r_{cavity} – the radius of the cylindrical cavity.

2.2.5 Beam-Tilt Design

RLSA antennas can also be used to produce tilted beams. Beam-tilt technique goals are to improve return loss problems and to produce a planar tilted wave. By producing a regular slot spiral, the boresight direction is at 0º and by producing a spiral with an elongated shape, the beam direction tilts accordingly. To place the slots in the right position, the following equations must be met. Each pair position is assigned with (ρ_i, φ_i) as previously described. The phase difference between slot pair and is given by [19]:

$$\rho_i(k_g - k_0 \sin\alpha_0 \cos\varphi_i), \tag{2.23}$$

where ρ represents the radial distance, k_0 and k_g are the wavenumbers in free-space and guided inside the PPW, respectively. α_0 is the angle chosen for the beam tilt and φ_i represents the azimuth of the slot pairs. To generate the spiral which will act as a base for slot placement we follow:

$$\rho_s(\varphi) = \frac{\varphi}{k_g - k_0 \sin\alpha_0 \cos\varphi} \tag{2.24}$$

From (3.2) and from k_0 and k_g:

$$k_0 = \frac{2\pi}{\lambda_0} \wedge k_g = \frac{2\pi}{\lambda_g}, \tag{2.25}$$

and

$$k_g = k_0 \sqrt{\epsilon_r} \tag{2.26}$$

The expression turns into:

$$\rho_s(\varphi) = \frac{\frac{1}{k_0\sqrt{\epsilon_r}}\varphi}{1 - \frac{\sin\alpha_0}{\sqrt{\epsilon_r}}\cos\varphi}, \tag{2.27}$$

and finally, to simplify:

$$\rho_s(\varphi) = \frac{a\,\varphi}{1 - b\cos\varphi} \tag{2.28}$$

Fig. 13 shows the difference between a standard spiral where $\alpha_0 = 0$ and an elongated spiral with $\alpha_0 \neq 0$ for tilted beam tilt design. The spiral on the left side becomes less spaced while on the right side, the distance increases and creates a stretched spiral shape.

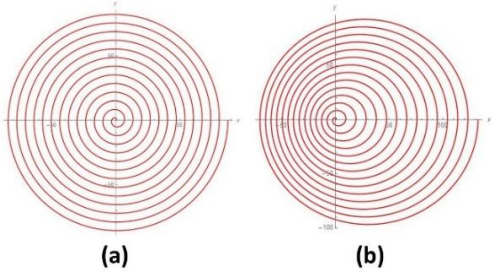

Fig. 13 – Difference between a standard spiral (a) and a spiral used for beam tilt (b)

The beam tilt unregular spiral shape poses a problem: the slots will be closer together on the left side, while on the right side they will be sparser. The slots must not overlap on the left side and cannot be too far apart on the right side. To ensure slot pairs in each arch are spaced accordingly a divide-and-conquer approach is devised. First, the spiral is divided into 8 parts. The angle value of the axes intersection with the spiral is then retrieved and we characterize each arch by 2 values: the angle at the start β_I, and at the end β_F. The number of pairs m is chosen for each arch. The difference between the arch angle of start and finish, represented by β_D, is divided by in equal parts, $m - 1$, to ensure an even and equidistant distribution. The following equations express the method:

$$\beta_D = \beta_F - \beta_I, \tag{2.29}$$

and

$$C = \frac{\beta_d}{m - 1}, \tag{2.30}$$

where C represents the angle between two pairs of slots in the same arch. This method is applied generally to all the arches. To finalize the process, some minor adjustments are made locally to sections 2, 3, 6 and 7 since the arches are less regular on those areas. Fig. 14 exemplifies the process described above.

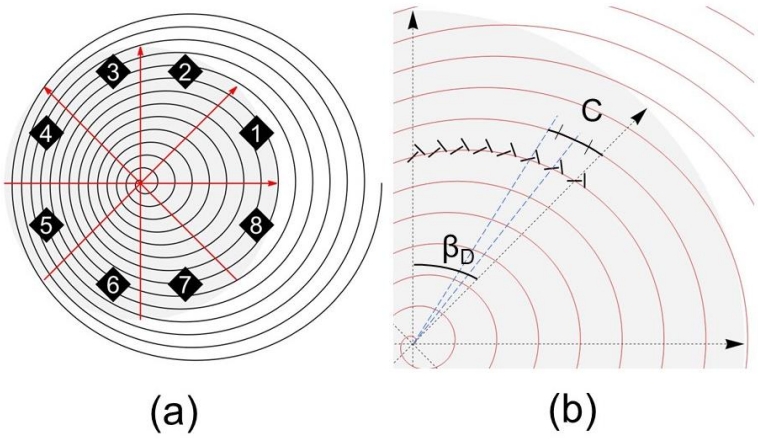

Fig. 14 – Method to fulfil slot pair distribution: Sectionalization of the RLSA into eight parts (a) and the method for positioning the slots in one single arch (b).

This method is not the more precise and needs further study and improvement. For a more precise distance between adjacent slot pairs, a mathematical model must be developed as in [19] or [27].

Chapter 3

Design and Simulation Results

RLSA antenna components and dimensions are studied in depth. The circular PPW structure is examined first using *CST STUDIO Suite*. Matching between the plates and coaxial feed is analysed looking at the distance between plates, its radius, and the depth at which the cable is inserted. An absorber rim is then considered to minimize the reflections at the perimeter of the structure and three materials are tested as filling between plates: air, Duroid 5880 and FR-4. After the study of the basic parts, focus is turned to slot dimension and distribution over the aperture. For slot dimension, a reduced model, one quarter of a RLSA, for multiple slot lengths is simulated and field behaviour observed before cutting all the slots in the top plate. For pre-prototyping the slots and their distribution, the developed GO/PO method develop in *Wolfram Mathematica* KH3Dslot is applied. In this manner, multiple hypothesis are tested before a full wave analysis in *CST STUDIO Suite* which can perform lengthy simulations.

3.1 Circular PPW design and optimization

3.1.1 Plates

For a better understanding of the plates, a study is made regarding its main parameters. The ones considered are plate radius, distance between plates and cables' core height inside the PPW and are referred as *rp*, *H* and *h_core,* respectively. Both bottom and upper plates, are given a 0.15 mm thickness and the coaxial cable for the excitation has 4.4mm of diameter. The materials used in the cable are copper for the core and PTFE (Teflon) for the dielectric surrounding the core. For the plates a PEC material is defined and the space between them is filled with air. Fig. 15 shows the model used for examining all the previous parameters.

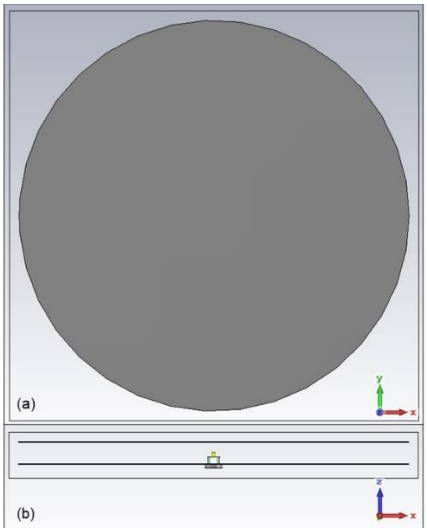

Fig. 15 – PPW model for simulation with plan view and side view, XY (a) and XZ (b) plans, respectively.

First, the radius is tested by running a simple simulation. The parameters *H* and *h_core* are kept constant, 2.5 mm and 2 mm, respectively and then we vary the radius. The reflections at the edges of the PPW are observed through $S_{1,1}$, which provides the behaviour for the amount of energy reflected back at the feed point for a certain frequency. Fig. 16 shows the result.

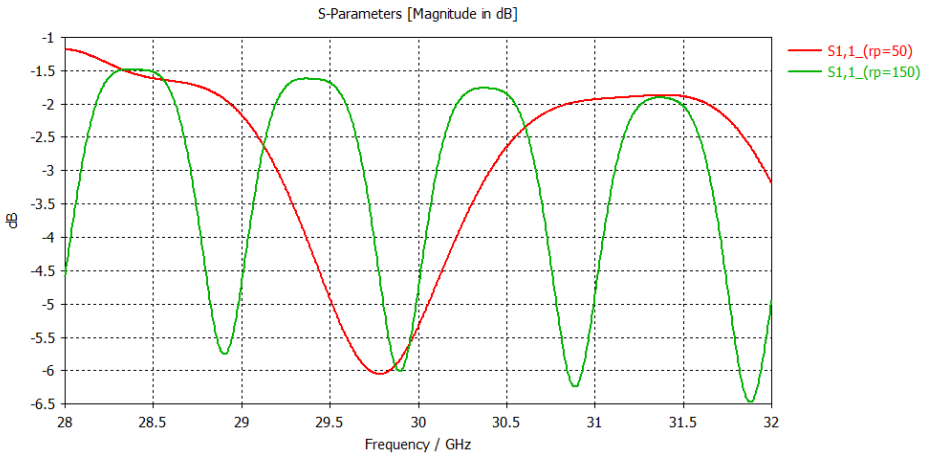

Fig. 16 – $S_{1,1}$ for *rp* = 50 mm (red) and *rp* = 150 mm (green). All for a PPW with the constant dimensions of *H* = 2.5 mm and *h_core* = 2 mm.

The dips in Fig. 16 are wider for a smaller radius. It also shows that with the radius increase the dips in $S_{1,1}$ become more frequent. A good match between PPW and feed is key to minimize undesired reflections. The advantage of one radius over the other comes from establishing a working frequency and tunning the structure around it to achieve a good antenna gain. The working frequency will affect directly slot length and consequently the number of slots that can be placed on the top plate. So, the radius should be established to achieve a particular gain value or to match a certain component dimension imposed.

For the next simulations we consider *H*, the distance between plates. PPW dimensions *rp* and *h_core* are kept constant, 150 mm and 2 mm, respectively while a sweep of H is made and $S_{1,1}$ is again examined. Fig. 17 points to the influence of *H* on internal reflections.

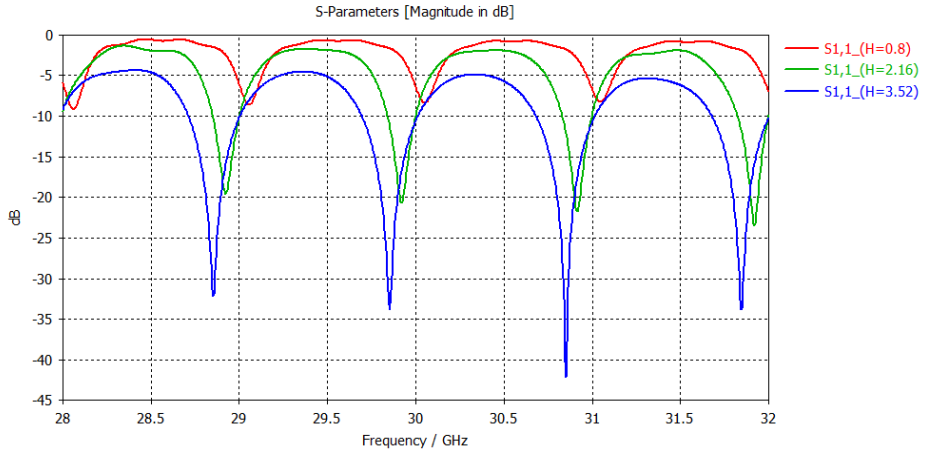

Fig. 17 – $S_{1,1}$ for *H* = 0.8mm (red), *H* = 2.16 mm (green) and *H* = 3.52 mm (blue). All for a PPW with the constant dimensions of *rp* = 150 mm and *h_core* = 2 mm.

A clear trend can be observed when analysing the graphic in Fig. 17. The bigger the distance between plates gets the less energy reflects back to the feed. The same periodic dips are observed consequence of running the simulation for a *H* = 150 mm, a behaviour stated before when increasing the radius.

For these simulations an H bigger than half wavelength is also contemplated simply to observe the higher modes of propagation inside the PPW. Three values of H are simulated. The first one is for an H = 4.5 mm, an example that follows equation (2.5) to generate only the fundamental mode $TM^{z}_{0,0}$. The next two examples are for H values higher than half wavelength, 7.5 mm and 10.5 mm. Fig. 18 shows the three circumstances.

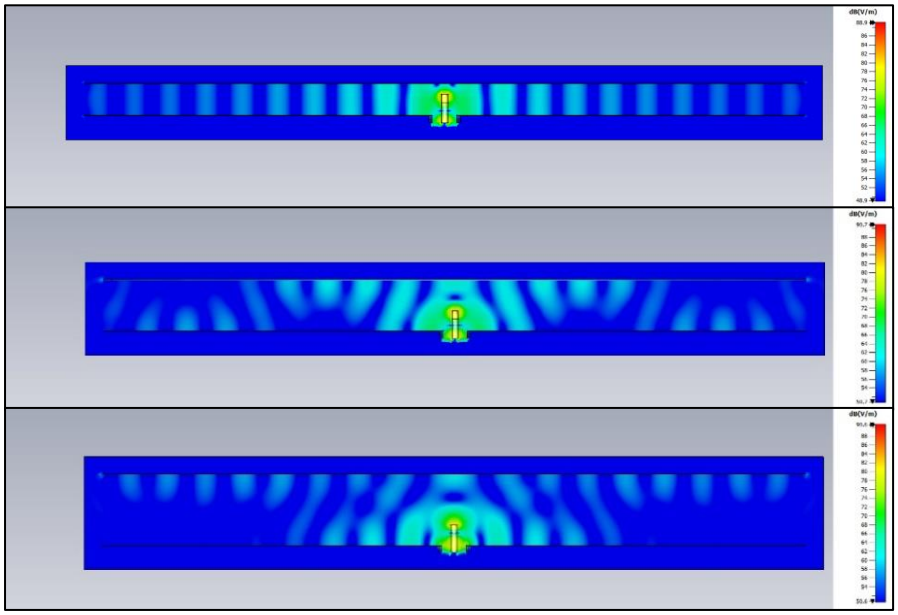

Fig. 18 – Magnetic Field on a PPW for H = 4.5 mm; 7.5 mm; 10.5 mm. All the above are for a *rp* = 50 mm and *h_core* = 2 mm

Naturally, amongst the observed fields, the first situation is the more beneficial solution: a uniform cylindrical wave propagating towards the edges of the PPW. The established condition referred to in theory is confirmed and for our final model, the expression (2.5) must be met.

Finally, to study the influence of coaxial cable depth inside the PPW, the same methodology is applied. By keeping *H* and *rp* constant, 2.5 mm and 150 mm, respectively, *h_core* is varied. Fig. 19 represents the $S_{1,1}$ results from the models.

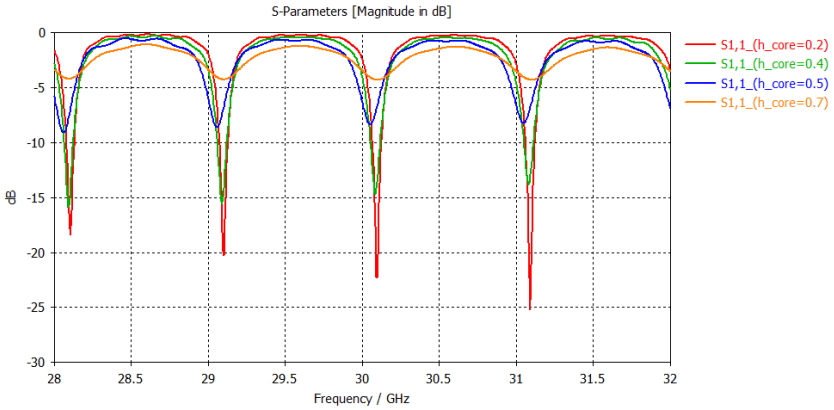

Fig. 19 – $S_{1,1}$ for *h_core* = 0.2 mm (red), *h_core* =0.4 mm (green), *h_core* = 0.5 mm (blue), *h_core* = 0.7 mm (orange). All for a PPW with the constant dimensions of *rp* = 150 mm and *H* = 2.5 mm

From Fig. 19, a clear trend emerges: the higher the core inside the PPW, the poorer the reflection coefficient $S_{1,1}$ becomes. The amount of energy reflected back at the feed also depends on the ability of the antenna to divert the energy at the end of the PPW. This can be achieved by placing an absorber at the end, a possibility which is explored in the next subsection, or when placing the slots on the top plate.

A better perception of tunning the PPW to reach the best reflection coefficient possible is the end goal of this subsection. The responsiveness of *rp*, *H* and *h_core* on the way they influence the PPW is obtained and is included in the next stages of design. For this work the objective is to achieve an antenna with 150 mm diameter, *rp* = 75 mm. Previous transmit arrays developed by the investigation group are of the same size.

3.1.2 Absorber rim

An absorber rim is introduced to contain the reflections for now, while there are no slots to leak the energy before it reaches the edge of the PPW. ECCOSORB AN-77 is chosen as the material for the simulations. Fig. 20 presents que AN-77 material at the edge of the structure.

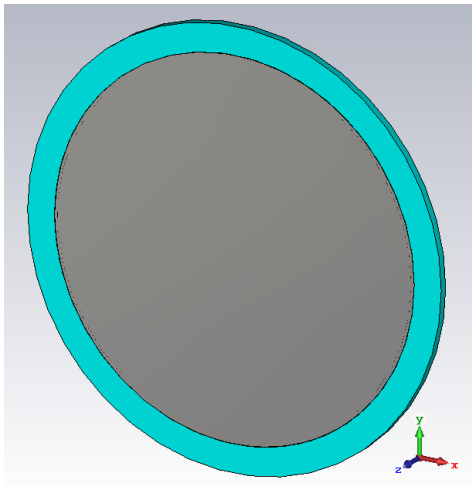

Fig. 20 – PPW model with a perimeter of ECCOSORB AN-77

The starting point for a fast analysis is reducing *rp*. A radius with 25 mm is set. By doing this, simulations will run faster, and an approximate result is obtained. A sweep is made between 5 mm and 15 mm when setting absorber rim thickness to see the effects on reflections back at the feed. Fig. 21 shows the result of this sweep for a frequency band of [29; 31] GHz. For an *H* = 3 mm and *h_core* = 2 mm, the best result occurs from a 10 mm thickness absorbent. This value happens to be λ_0, free-space wavelength for 30GHz, meaning the absorber rim dimensions should be set corresponding to a wavelength measure of the target frequency.

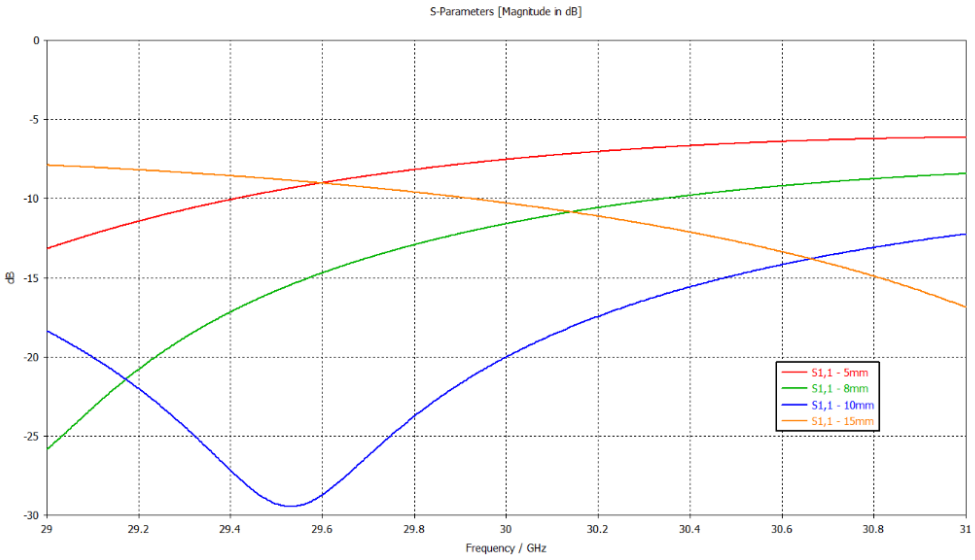

Fig. 21 – $S_{1,1}$ for ECCOSORB AN-77 thickness of 5 mm (red), 8 mm (green), 10 mm (blue) and 15 mm (orange). All the variations are simulated with an *H* = 3 mm and an *h_core* = 2 mm.

To see the effects on wave propagation inside the PPW, two different cuts of the structure are compared. Fig. 22(a) presents a PPW without with no termination at the perimeter and Fig. 22(b) shows a PPW with a 10 mm ECCOSORB AN-77 termination. Both examples present a 30dB scale between maximum and minimum value.

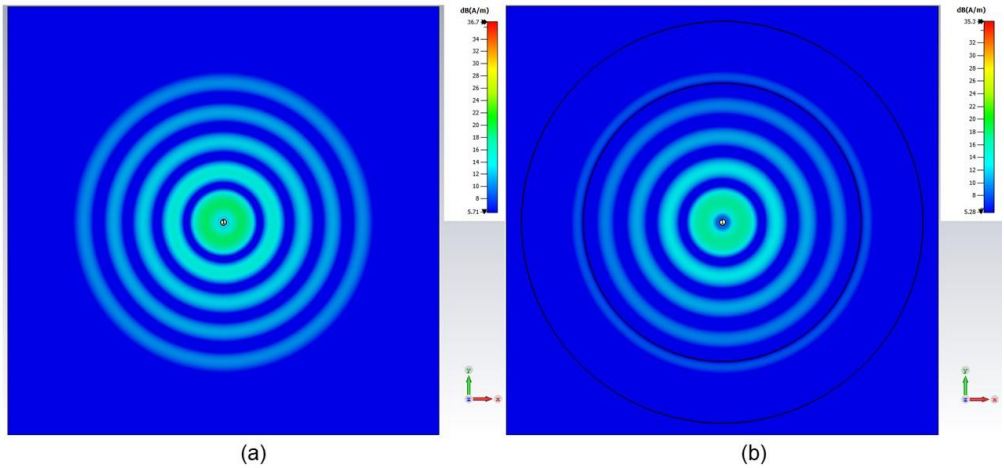

Fig. 22 – f = 30GHz Magnetic Field (dBA/m) plan view: (a) no absorber rim and (b) ECCOSORB AN-77 with 10mm. Both examples have *rp* = 25mm, *H* = 3mm and *h_core* = 2mm.

Although it is not very visible, the fields at the termination weaken and are less intense near the feed when comparing Fig. 22(b) to Fig. 22(a). Also, by comparing the scales, a difference of 1.4dB arises between the two field cuts. By analysing $S_{1,1}$, a visible distinction is noted. There is a significant reduction in reflections back at the feed when using ECCOSORB AN-77. This means the excess energy that reached the end of the PPW is not reflected back but rather absorbed. Fig. 23 compares both cases.

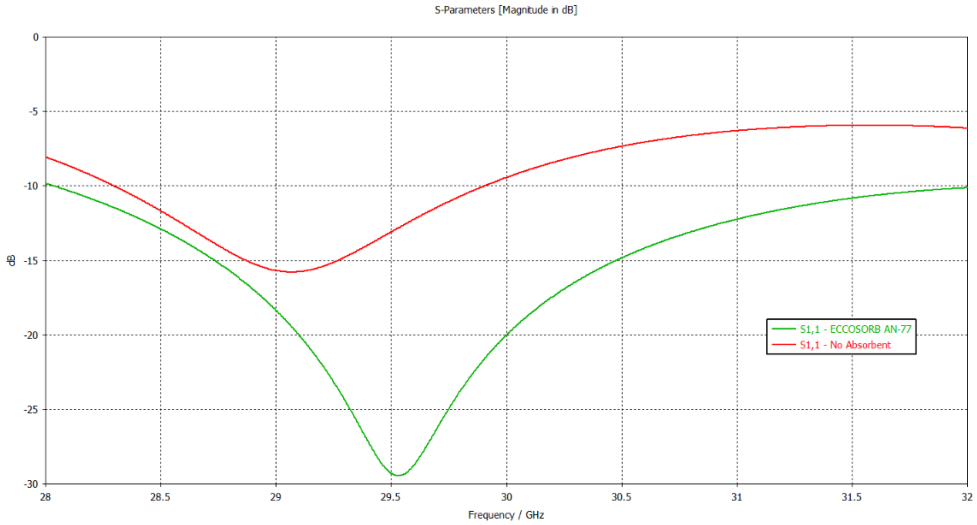

Fig. 23 – $S_{1,1}$ for no absorbent (red) and ECCOSORB AN-77 with 10mm (green). Both examples have *rp* = 25 mm, *H* = 3 mm and *h_core* = 2 mm.

To confirm the method and the feasibility of working with a smaller model, an expansion is made for *rp* = 75mm. The model is simulated with both *H* = 2 mm and *H* = 1.5 mm and because of this reduction *h_core* is also smaller, *h_core* = 1 mm. By looking at Fig. 24, which gives us $S_{1,1}$ for both values of H, verify a slight shift in frequency. Although the minimum value differs in 5dB, when comparing with Fig. 23, it is still below the desired threshold of -10dB.

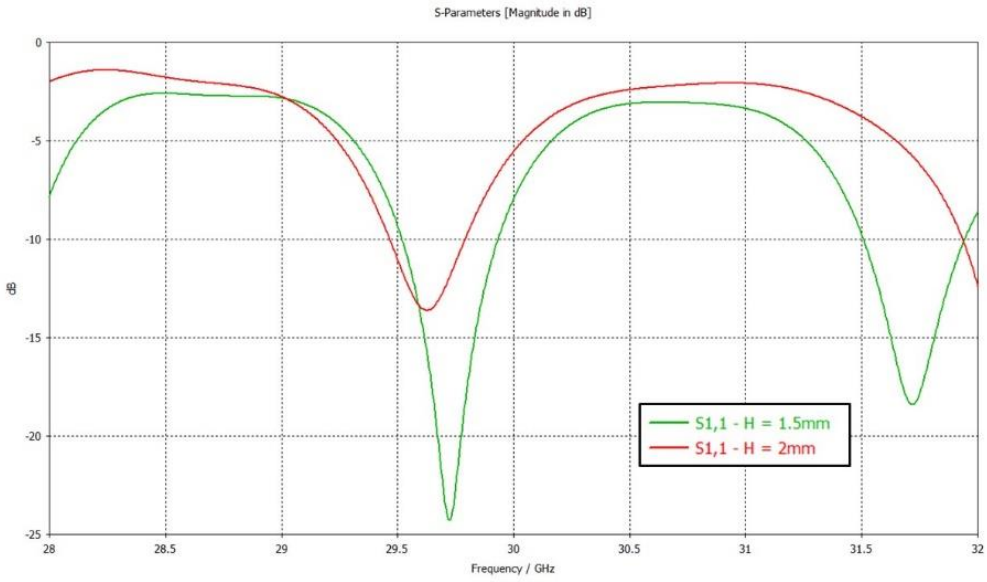

Fig. 24 – $S_{1,1}$ for a PPW with *rp* = 75mm and *h_core* = 1mm: *H* = 2.0mm (red) and *H* = 1.5mm (green)

For a final confirmation, magnetic field magnitude is observed to make sure wave propagation inside the PPW is ideal. A similar cylindrical wave is present inside just as depicted for a PPW of *rp* = 25mm and it can be seen in Fig. 25.

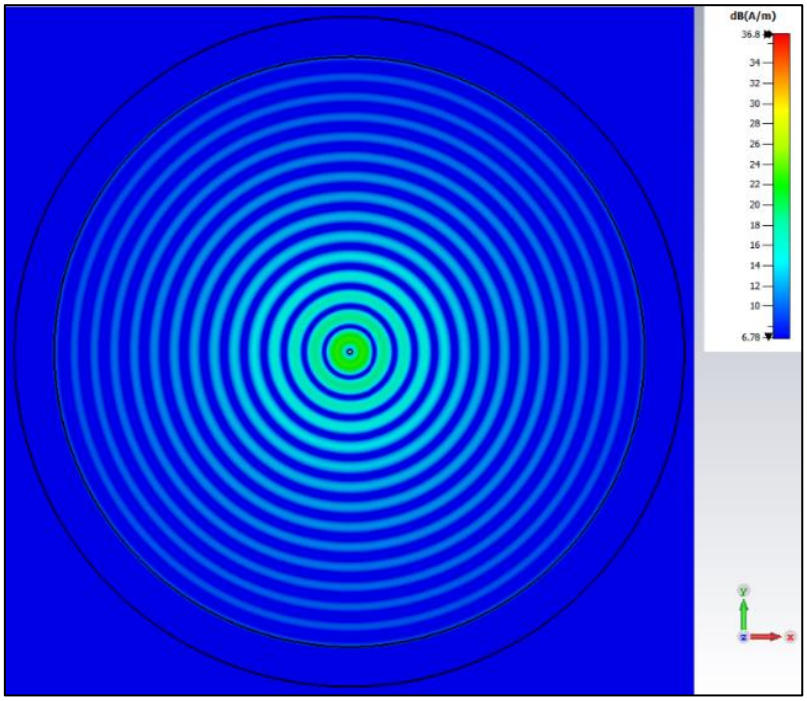

Fig. 25 – Magnetic field (dBA/m) for a PPW with rp = 75 mm, H = 1.5mm and h_core = 1 mm.

3.1.3 Dielectric Substrates

On the next step, the option of filling the inside of the PPW with a dielectric substrate is studied. A dielectric substrate is depicted in Fig. 26. Duroid 5880 and FR-4 are the materials tested. Duroid 5880 has a relative electric permittivity of ε_r = 2.2 and FR-4 ε_r = 4.4. This effort is made to shorten the wavelength. By doing so, an improvement is expected for energy performance of the structure since the distance between points with the same phase will be closer and thus, slots will be placed closer and in higher number. More on how substrate influences distributing slots over the aperture and sizing them is explored in Section 3.2.

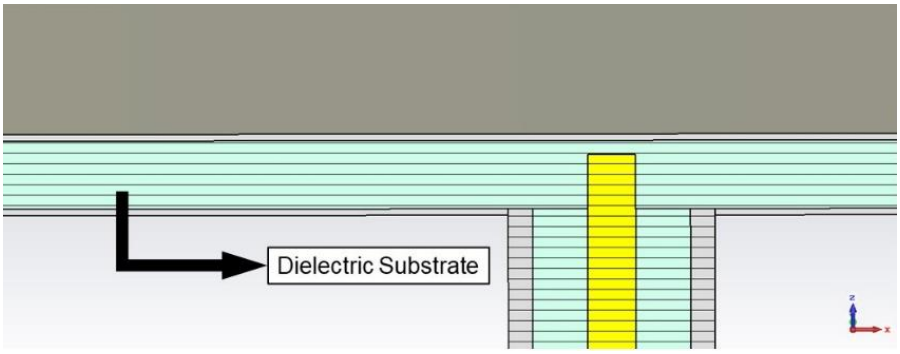

Fig. 26 – PPW model with a substrate filling between plates.

According to equation (2.6), the guided wavelength is no longer considered to be free-space wavelength if a substrate is added. Table I shows the guided wavelength for each dielectric material based on their ε_r and it is noted that an increase of electric permittivity, implies a decrease in guided wavelength.

Table I – Guided Wavelengths for different dielectric materials: air, Duroid 5880 and FR-4.

	Air ($\varepsilon_r = 1.0$)	Duroid 5880 ($\varepsilon_r = 2.2$)	FR-4 ($\varepsilon_r = 4.2$)
λ_g [mm]	10	6.74	4.87

To compare substrates, several simulations are made to monitor internal reflection and field behaviour for the established *rp* = 75mm and a number of h_core values. Fig. 27 only shows one of the best values obtained for both substrate, h_core =1.25 mm. For H, air and FR-4 simulations are kept at H=1.5mm while for Duroid 5880 a slighty higher value is considered, H=1.575 mm, since it is the thickness available in the laboratory.

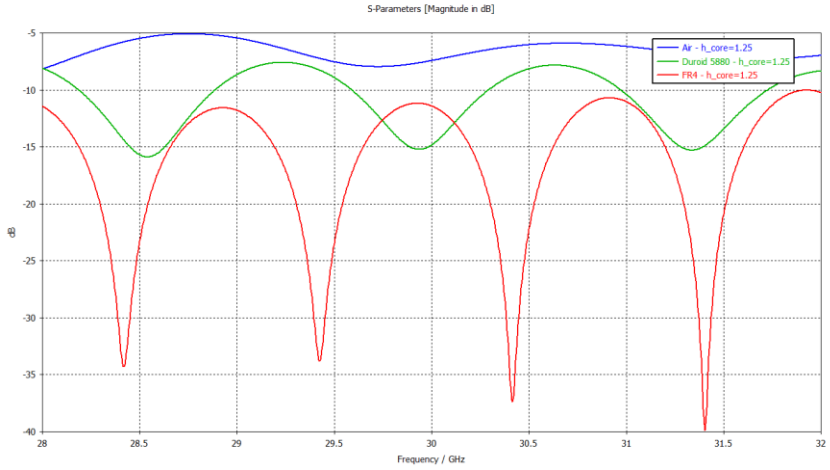

Fig. 27 – $S_{1,1}$ for a PPW with *rp* = 75 mm and *h_core* = 1.25 mm and different dielectric substrates: Air H = 1.5 mm (blue), Duroid 5880 H = 1.575 mm (green) and FR-4 H = 1.5 mm (red)

By evaluating the three curves in Fig. 27, both substrates outperform an air filled PPW and Fr-4 presents far greater dips than Duroid 5880. In Fig. 28, as indicated in Table I, the reduction of the guided wavelength is visible: FR-4 creates the shorter wavelength. The possibility of using any of these materials needs further analysis because there are other factors to take into consideration. Slot dimensions and slot distribution are the main factor of this work. For the next section, an evaluation is performed on how the fields represented in Fig. 25 and Fig. 28 are affected and how do they compare with each other.

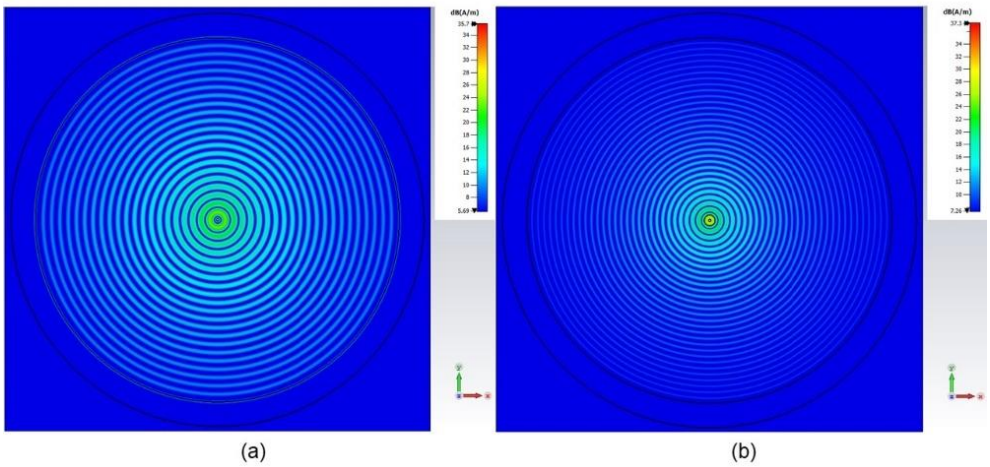

Fig. 28 – f = 30GHz Magnetic Field (dBA/m) plan view: (a) Duroid 5880 and (b) FR-4. Under the same conditions as described in Fig. 27.

3.2 Aperture design

From the results so far, it is understood that adjustments to the coaxial cable leads to a better frequency tunning but, how the fields will behave once the slots are placed has not been contemplated. When slots collimate the wave in the waveguide, they interfere with the fields inside and this disruption can also contribute to more energy reflected back at the feed. In turn, some more tweaks need to be made in the cable because the fields are no longer the same as seen in the previous section. Therefore, to guarantee the levels of $S_{1,1}$ are in line with the defined standard and that antenna gain, and efficiency perform accordingly, the slot dimensions and aperture distribution are examined closely in this section to fit the dimensioned PPW. KH3Dslot and CST results are compared.

3.2.1 Slot dimensions

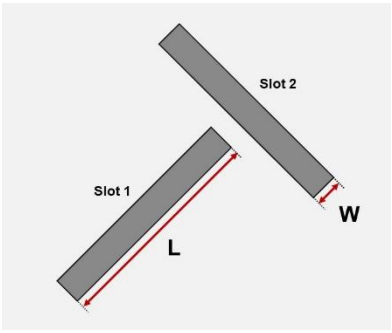

Fig. 29 – Slot pair dimensions: L – Length [mm] and W – Width [mm]

For an in-depth study on slot dimensions, as represented in Fig. 29, and how it affects performance, multiple simulations run in *CST Studio Suite*. These tests consist of a structure modelled after a quarter of a PPW and of a single slot pair place upon the top plate. An absorbing material, ECCOSORB AN-77, is placed at the edge to minimize reflected wave disturbances to the field that may occur. Additionally, to feed the structure, a discrete wave port is placed at the origin of the structure to

carry out excitation and, the open-ended sides boundaries magnetic fields in planes YZ and XZ are null. By doing so, a quarter of the radial wave is synthesized, and the slot pair collimates the guided wave as if the full PPW was present. The pair radial distance is varied, from λ_g to $7\lambda_g$, and the length of the slots is also varied in the interval [3.0; 7.5] mm with a sampling step of 0.5 mm. Slot width is kept constant throughout the process, W = 0.5 mm.

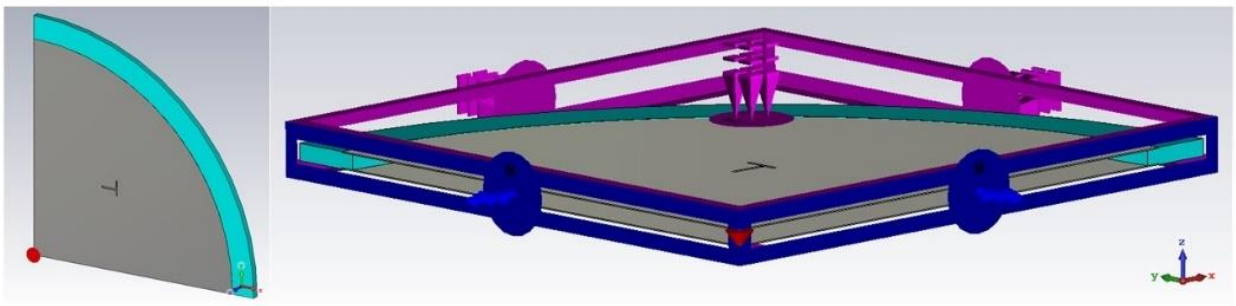

Fig. 30 – Slot dimension study model in *CST STUDIO Suite:* one quarter of a PPW with a single slot pair on top

For the tests, distance between plates is 2mm and structure radius is held at 75 mm, equal to *rp* from the full RLSA. Electric and Magnetic fields are monitored by measuring their values at the middle of each slot. All the simulations are at 30 GHz. Then, an average between recorded values of each field in each slot (Slot 1 and Slot 2 as in Fig. 29) is calculated. The results are plotted, and the best fitting function calculated. Fig. 31 shows an example for the result of these steps.

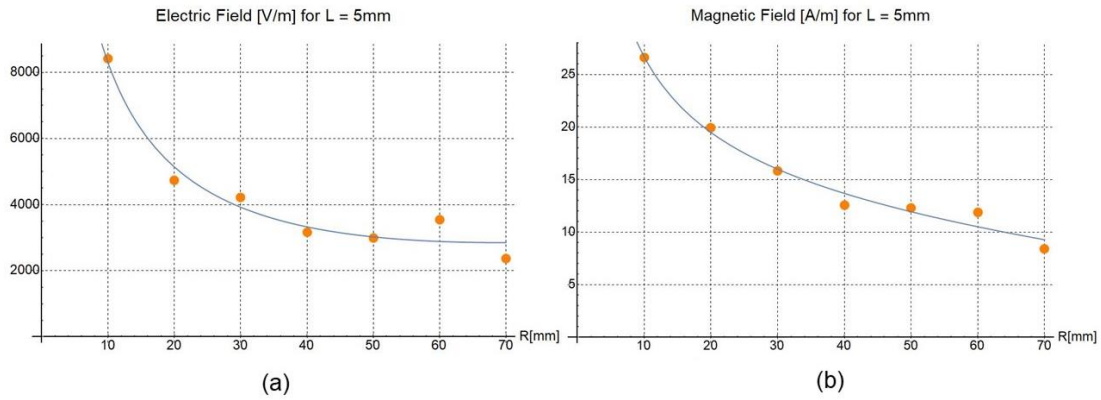

Fig. 31 – Average electric (a) and magnetic (b) fields at the centre of the slots as a function of the radial distance

When assessing Fig. 31, it is noticed the fields radiated at each sample over the radial line resemble Fig. 32, a plot of $\frac{1}{\sqrt{\rho}}$. This can be explained by equation (2.9) which establishes Hankel function asymptotic approximation of the fields inside a circular PPW. Electric and magnetic fields are inversely proportional to the radial distance square root hence, the radiated fields through the slot pair will behave the same way.

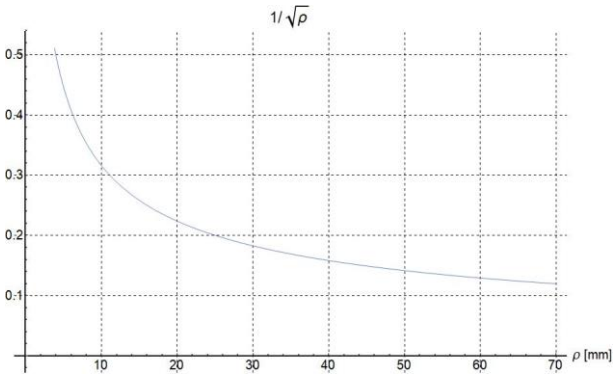

Fig. 32 – Plotted function of $\frac{1}{\sqrt{\rho}}$

For all the tested cases the wavelength becomes λ_0 because the wave propagates through air. The results for all the slot length and radial distance variations tested are shown in Fig. 33 and Fig. 34. Similar radiated field results are presented but with different levels. Slot with a length of 4.0 mm, 4.5 mm, 5.0 mm, and 5.5 mm seem to perform better. As the length gets closer to half guided wavelength $\frac{\lambda_0}{2}$, the fields are greater, meaning the length becomes more resonant with the fields. With this in mind, for the following parts of this work each slot length is L = $\frac{\lambda_g}{2}$. Additionally, slot width is kept in line with this experiment. If for an air filled PPW the width is 0.5 mm, it means it is 20 times lower than λ_0. As a result, a generalization is made from now on, W = $\frac{\lambda_g}{20}$, making the initial set value for width dependent on the guided wavelength.

A main concern with this single slot pair approach in a reduced structure is the likelihood of this method actually reproducing the performance of a slot pair in a fully completed RLSA antenna. It may in fact be too simplistic because adjacent pairs in a spiral array may have influence on each other. After an initial value for L and W are set slot distribution becomes the focus. This process is discussed in the next section.

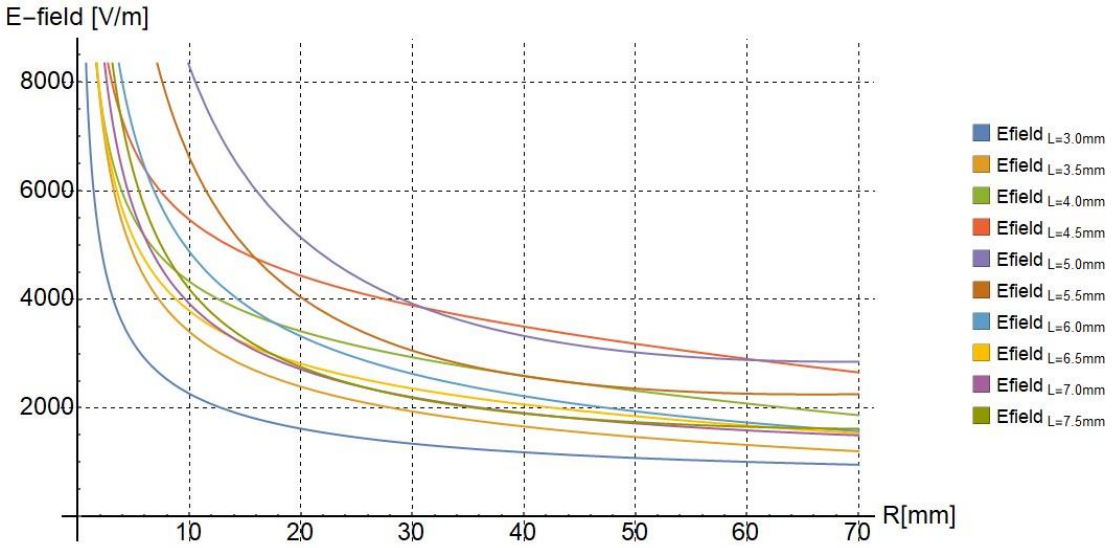

Fig. 33 – Electric fields [V/m] for slot length ∈ [3.0;7.5]mm as a function of radial distance.

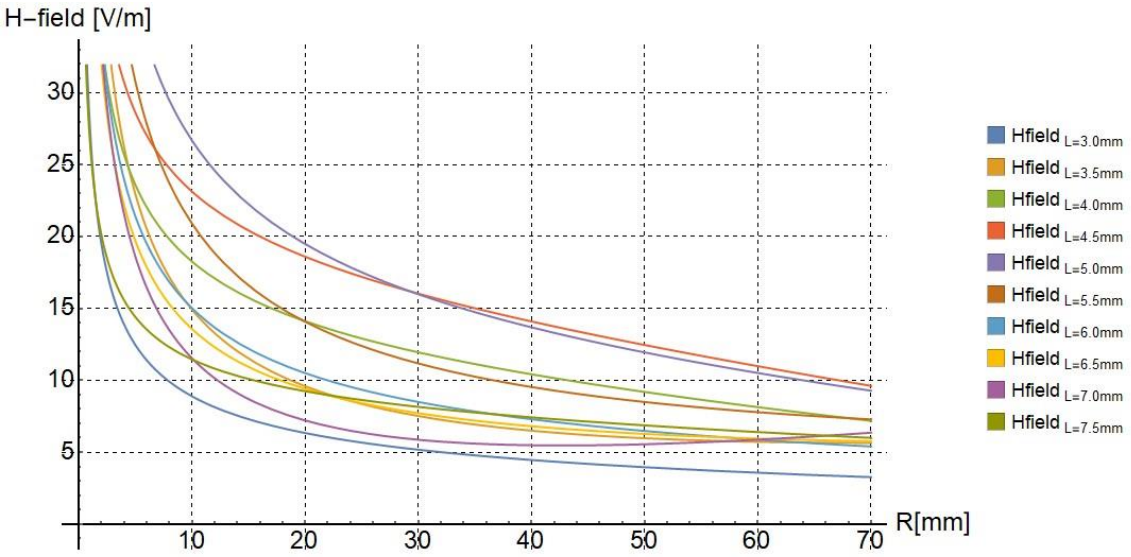

Fig. 34 – Magnetic fields [A/m] for slot length ∈ [3.0;7.5]mm as a function of radial distance.

3.2.2 Slot distribution

To define the distribution parameters, the substrate needs to be chosen. It as a direct influence on the guided wavelength as stated earlier that in turn has a direct effect on how the slot pairs will be sized and how they will be spaced. For a fast study on the effects of a dielectric substrate, KH3Dslot [46] is used. From the script directivity and farfield cuts are obtained and compared.

First, a one turn spiral for RLSA with no substrate and starting at a distance of $2\lambda_0$ from the centre is created, as seen in Fig. 35(a). The same is applied for Duroid 5880 and FR-4 but this time starting an equivalent $2\lambda_g$ depending on the dielectric. Instead of having a single turn spiral for each case, the apertures for substrate testing are equivalent in radius and in area, both end at the same radial distance as the first spiral. By guaranteeing the same area, a more accurate and fair comparison can be made between the materials. Fig. 35(b) and Fig. 35(c) represent the slots for Duroid 5880 and FR-4, respectively. All the slots in KH3Dslot are arranged to produce LHCP.

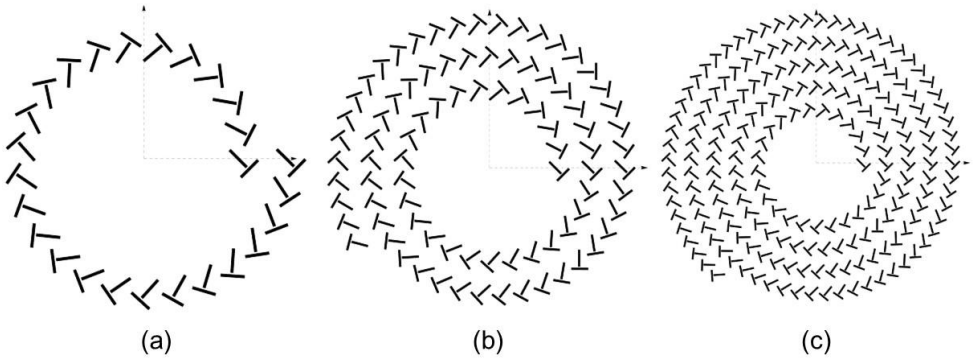

Fig. 35 – Equivalent slot spirals for different materials: air (a), Duroid 5880 (b) and FR-4 (c)

The results of this comparison are detailed in Table II. A visible improvement in Directivity is visible by using one of the substrates. There is a small difference of 0.8 dB between Duroid 5880 and FR-4 but there are other things to factor in before a choice is made.

Table II – Slot, spiral and directivity results comparison between substrates

	Air ($\varepsilon_r = 1.0$)	Duroid 5880 ($\varepsilon_r = 2.2$)	FR-4 ($\varepsilon_r = 4.4$)
$L = \lambda_g/2$ [mm]	5	3.37	2.38
$W = \lambda_g/20$ [mm]	0.5	0.337	0.238
S_φ [λ_g]	0.62		
Spiral start = $2\lambda_g$ [mm]	20	13.48	9.53
Spiral end [mm]	32.5		
Dir. [dB]	18.4	23.2	24.0

KH3Dslot also shows three-dimensional radiation patterns and LHCP and RHCP farfield cuts for φ = 90º or φ = 0º plane. Since the slots are arranged for LHCP, a LHCP comparison farfield cuts is made in the φ = 90º plane. Fig. 36 shows the farfield cuts in the φ = 90º for LHCP.

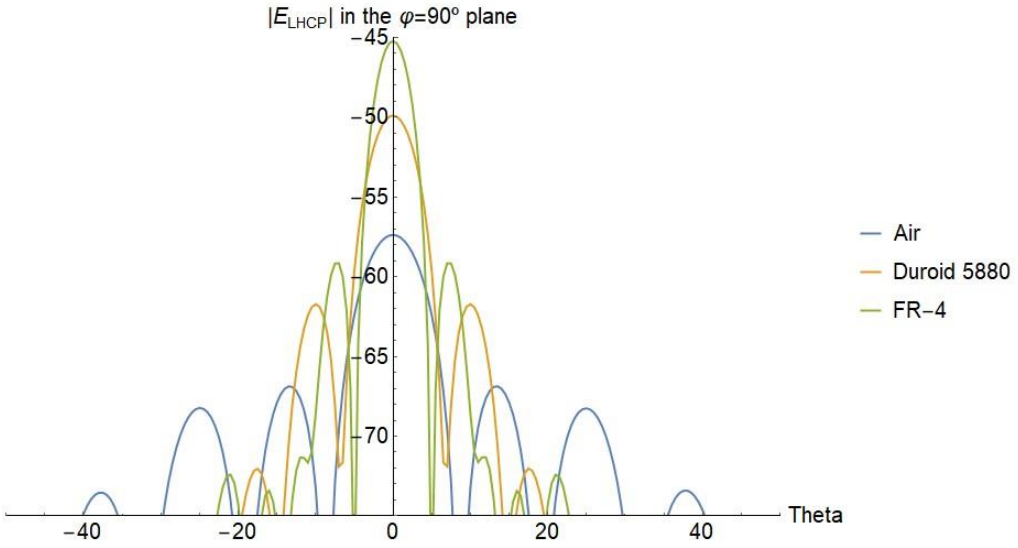

Fig. 36 – Electric farfield cuts in φ=90º plane for different materials: air (blue), Duroid 5880 (orange) and FR-4 (green).

It is clear from Fig. 36, the number of secondary lobes decreased by considering a dielectric substrate and the main lobe becomes more directive. Moreover, SLL (Side Lobe Level) is also reduced. FR-4 has the best performance form all the materials followed by Duroid 5880.

Further study for the materials is needed since KH3Dslot does not account for efficiency or internal reflections. A full-wave analysis in *CST STUDIO Suite* is used to confirm KH3Dslot results and provide the missing information. The analysis is conducted at 30 GHz and with the same slot dimensions and distribution parameters that are set in Table II. Since KH3D does not account for reflections, an absorbent is placed to approximate both models. The cable is positioned with an h_core = 1.25 mm and

slots are oriented to perform RHCP. Fig. 37 shows the models created in *CST STUDIO Suite*.

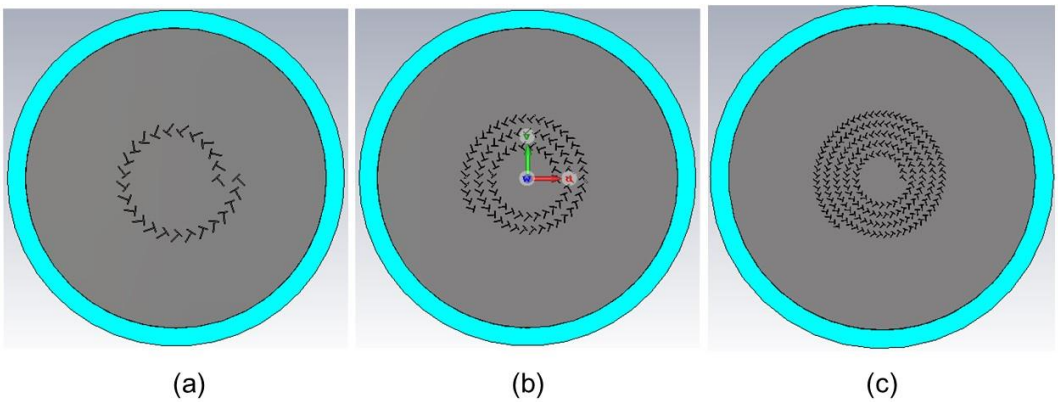

Fig. 37 – Equivalent slot spirals for different dielectric materials in *CST STUDIO Suite*: air (a), Duroid 5880 (b) and FR-4 (c)

Fig. 38 details $S_{1,1}$ results for these three simulations. As it was previously seen in section 3.1.3, where the PPW filling is analysed with no slots, dielectric materials have a great influence on internal reflections. $S_{1,1}$ is lower for an air filling, followed by Duroid 5880 and at last by FR-4. In these cases, with a small area of the top plate covered with slots, effects on lowering the $S_{1,1}$ parameter contrast with Fig. 27 in section 3.1.3. FR-4 might be favoured previously while on the current route it underperforms. Duroid 5880 roughly maintains its levels of internal reflections and air reduces $S_{1,1}$ levels when comparing to Fig. 27. This shift in material performance can be related to the increase of openings in the top plate. A greater number of slots covering the antenna means a higher perturbance of the guided wave and thus, an increase of reflections back at the feed. Duroid 5880 and air are likely to be the better choices for the substrate.

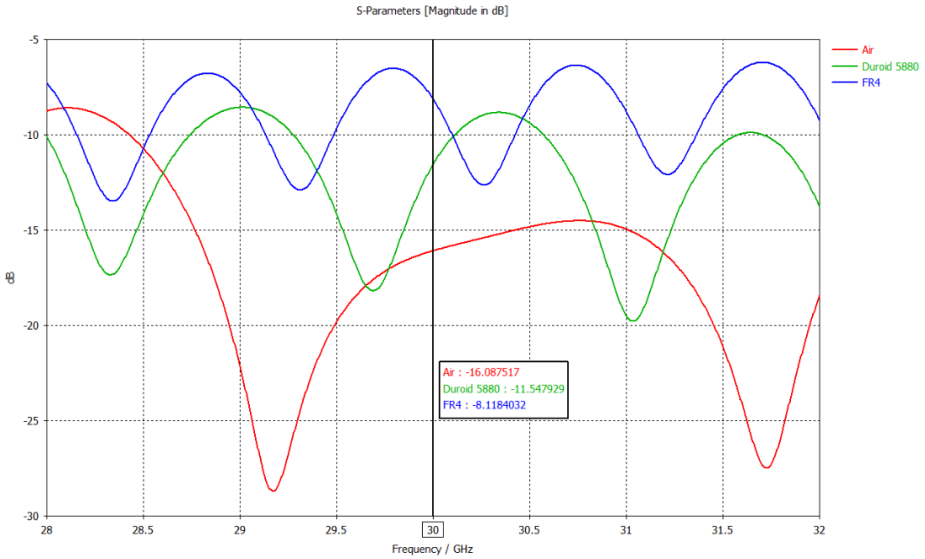

Fig. 38 – $S_{1,1}$ for each structure in Fig. 37: Air (red), Duroid 5880 (green) and FR4 (blue)

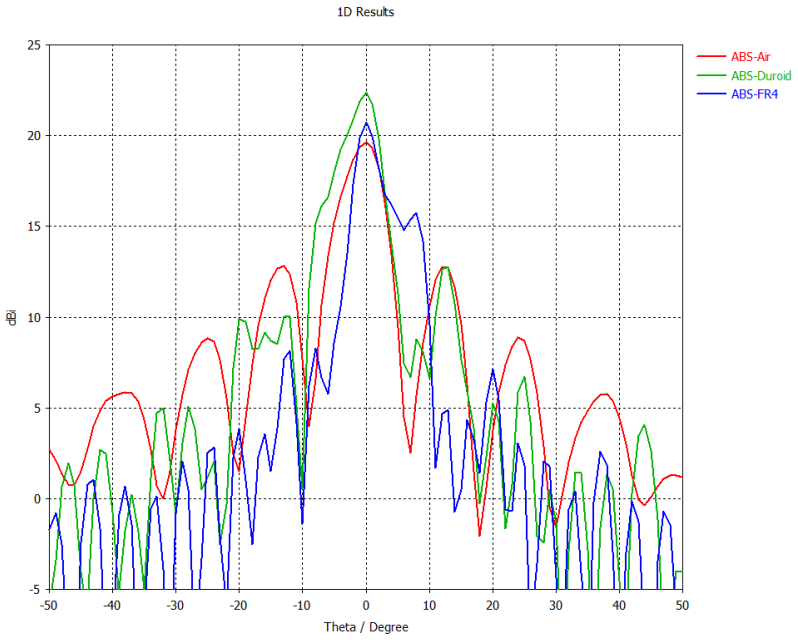

Fig. 39 – Electric farfield cuts in CST STUDIO Suite for φ = 90º plane for different materials: air (red), Duroid 5880 (green) and FR-4 (blue).

Other outcomes are evaluated to choose the substrate. Directivity, cross polarization level and efficiency are considered to weight all the compromises. Table III presents the values of said results and the H at which each simulation is carried out.

Table III – *CST STUDIO Suite* Partially filled aperture results comparison using multiple substrates @ 30 GHz

	Air ($\varepsilon_r = 1.0$)	Duroid 5880 ($\varepsilon_r = 2.2$)	FR-4 ($\varepsilon_r = 4.4$)
H [mm]	1.5	1.575	1.5
Dir. [dB]	19.6	22.4	20.7
$S_{1,1}$ [dB]	-16.1	-11.5	-8.1
X-POL [dB]	-13.4	-29.7	-11.7
Rad. Efficiency [dB]	-0.5	-4.7	-5.7

After examining Table III a decision is made regarding further material testing. It is noticed for both FR-4 and Duroid 5880 substrates radiation efficiency and $S_{1,1}$ are smaller in contrast with air, with the latter being the lower of all three cases. FR-4 has the lowest X-Pol levels and the increase in directivity is small. Duroid 5880 presents the highest directivity and best X-Pol levels of all the three. Air presents the best values for radiation efficiency and $S_{1,1}$. Based on the analysis, FR-4 is discarded from further examination while Duroid 5880 and air continue to be considered. While Duroid 5880 has a smaller radiation efficiency than air, it also achieves a better directivity. It is a necessary compromise to factor in to improve RLSA antenna directivity. Furthermore, looking at Fig. 38 Duroid 5880 also shows manageable levels of $S_{1,1}$ which can re-tuned and improve with future optimizations. The latter is also available for prototype construction and is widely used by authors in the multiple authors for this type of application.

Although there is a small difference between directivity values of Table II and Table III, there is a good enough agreement between KH3Dslot script and CST STUDIO Suite to expand testing. A comparison between Fig. 36 and Fig. 39 confirms the radiation pattern resemble each other. Secondary lobes are comparable for both GO/PO method and the full-wave analysis, but the main difference resides on the main lobe shape. For a full-wave analysis using CST STUDIO Suite does not use an asymptotic formulation thus, it is expected a slight difference in results.

With two options left, two fully completed RLSA antenna are tested: air and Duroid 5880. Two apertures are generated with KH3Dslot before moving to a full wave analysis. Fig. 40 represents both slot pair distributions for air and Duroid 5880. The slot dimensions and azimuth distance remains as presented in Table II. Both spirals start at $2\lambda_g$ and end right before *rp* = 75 mm.

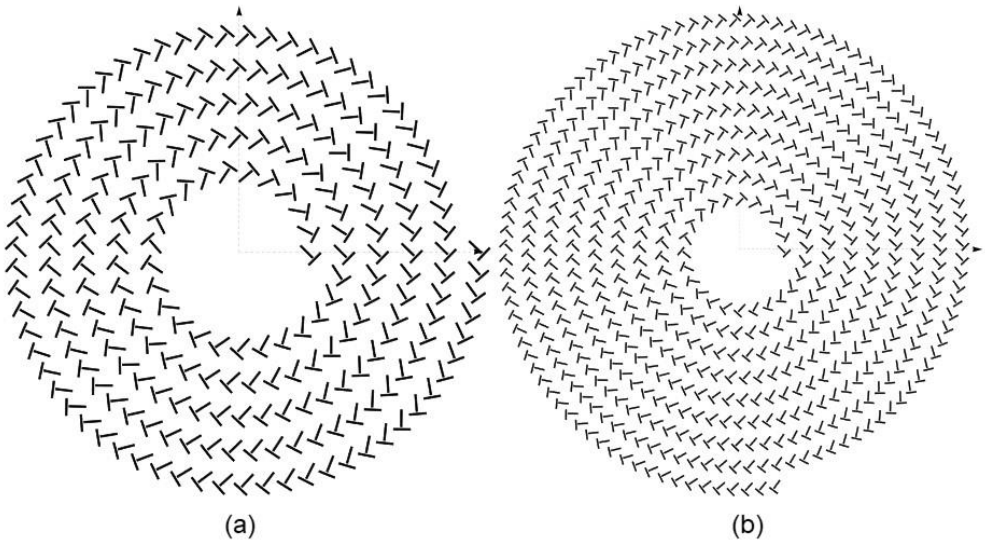

Fig. 40 – Complete RLSA aperture layout for air (a) and Duroid 5880 (b) in KH3Dslot

Table IV – Complete RLSA aperture directivity [dB] result in KH3Dslot

	Air ($\varepsilon_r = 1.0$)	Duroid 5880 ($\varepsilon_r = 2.2$)
Dir. [dB]	26.5	29.4

Table IV shows the directivity values for both apertures shown in Fig. 40. Using Duroid 5880 material improves the directivity relative to air, as it is expected. *CST STUDIO Suite* is used to complement and confirm the results given by KH3Dslot. The simulations are set with the same parameters defined previously for reduced aperture simulations. Fig. 41 shows the software created models and Table V the corresponding results.

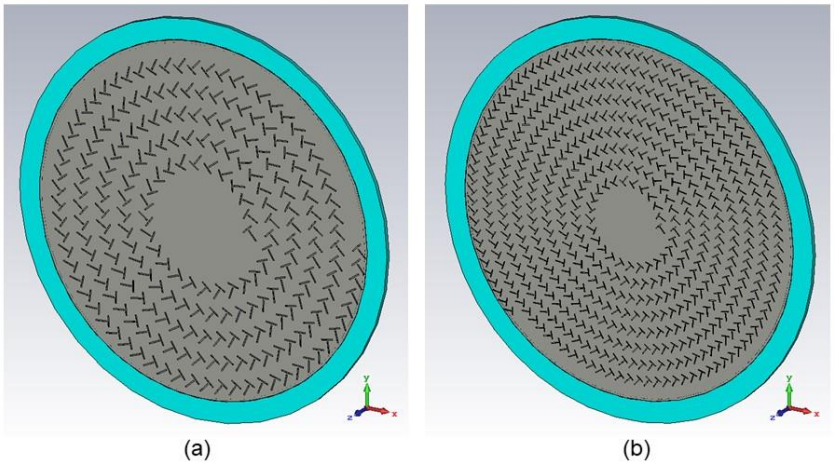

Fig. 41 – Complete RLSA model for air (a) and Duroid 5880 (b) in *CST STUDIO Suite*

Table V – *CST STUDIO Suite* RLSA antenna results comparison using air and Duroid 5880 @ 30 GHz

	Air ($\varepsilon_r = 1.0$)	Duroid 5880 ($\varepsilon_r = 2.2$)
H [mm]	1.5	1.575
Dir. [dB]	22.25	29.35
$S_{1,1}$ [dB]	-4.85	-12.54
X-POL [dB]	-23.0	-13.11
Rad. Efficiency [dB]	-0.11	-2.72

Table IV and Table V show a good agreement in directivity since they appear to be in the same order of magnitude. Some variations occur because of formulation limitations in KH3Dslot script. It is confirmed that using a material with higher electric permittivity will increase RLSA antenna directivity. Looking at the other findings in Table V, $S_{1,1}$ at 30 GHz improves when using Duroid 5880 but X-Pol levels increase. This X-Pol level increase may derive from the rise in slot numbers since the results for a partially filled RLSA in Table III present lower levels. Fig. 42 shows $S_{1,1}$ comparison for both Air and Duroid 5880.

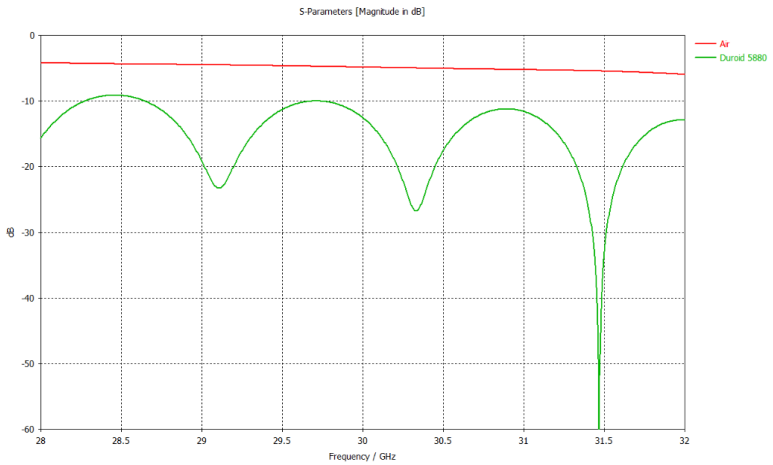

Fig. 42 – $S_{1,1}$ for a complete RLSA: Air (red) and Duroid 5880 (green)

Duroid 5880 is chosen to be placed inside the RLSA antenna but for the tested frequency of 30 GHz, efficiency is not the best to be achieve. A compromise is made to increase a better directivity and a reduced level of internal reflections. Varying the initially established slot dimensions and spacing can counteract the poor efficiency. It is also understood that by doing so the slots will be detuned from the preferred frequency of 30 GHz. In parallel with this new dimension variation, a frequency sweep is performed around 30 GHz to find a better suited working frequency.

The first adjustment is made concerning the position of the slots: the radial distance of every slot pair is shortened by an eight of the guided wavelength as show in Fig. 43. The positioning is applied in [34]. This way, the centre of the first pair of each spiral turn is on top of the field maximum. In preceding simulations, only the first slot of the pair centre is on top of the field maximum. Such small change as a small effect on performance but allows to place a few more slots on the top plate.

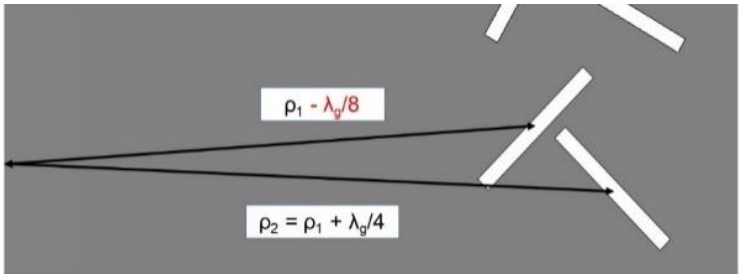

Fig. 43 – Radial adjustment for the slot pairs

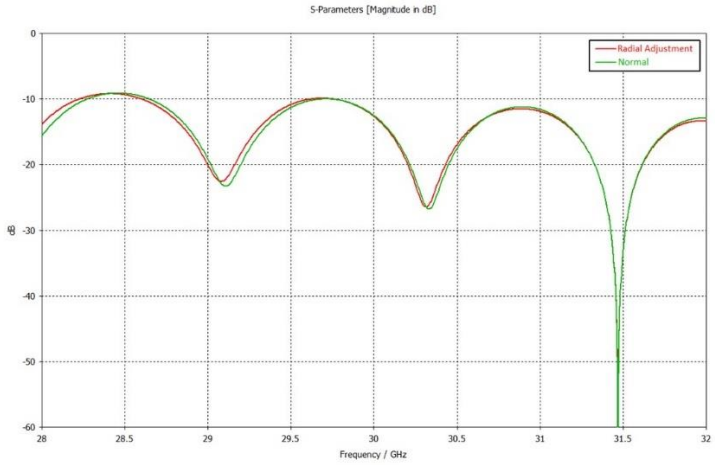

Fig. 44 – $S_{1,1}$ for a complete RLSA: before the radial adjustment (green) and after the radial adjustment (red)

Through a full wave analysis in *CST STUDIO Suite* small effects can be seen. No significant change on internal reflections is visible because $S_{1,1}$ practically the same as before. Fig. 44 represents $S_{1,1}$ for both cases, before and after the change. As for the antenna directivity it remains the same with a reduction of SLL. The main lobe becomes larger and more regular with this small adjustments. Fig. 45 shows the beam shape and directivity comparison of both cases. These changes are maintained for future simulations.

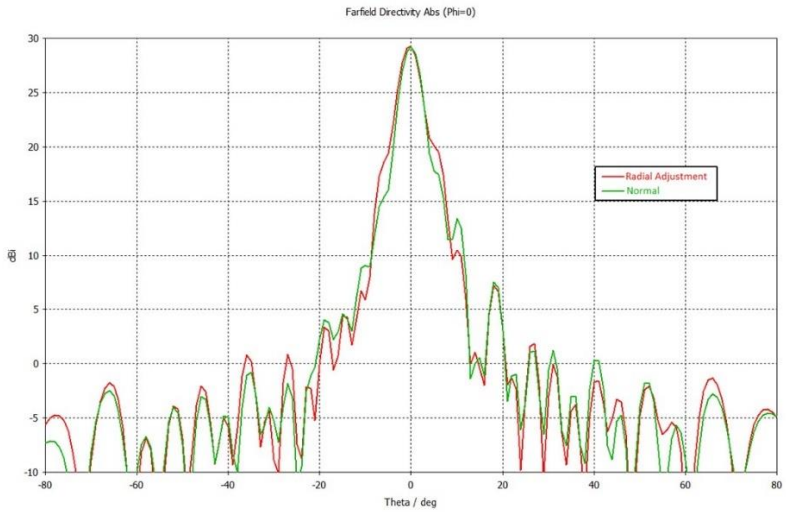

Fig. 45 – Beam shape and Directivity comparison for 2 completed RLSA: before the radial adjustment (green) and after the radial adjustment (red)

The second modification to achieve better performance is changing the slot dimensions, L and W. A parameter sweep is made for both values. For length, the simulations start at the previously established L = $\frac{\lambda_g}{2}$, which is 3.37 mm and stop at around 3.8 mm. Length cannot be increase further because the modelled slots may intersect. For width, follows an equal path. It starts at W = $\frac{\lambda_g}{20}$, which is 0.337 mm and stops at 0.6 mm. Width cannot be larger because field components may appear in undesired directions, which can cause an increase of cross-polarization level.

At the end of the sweep best results are found at 28.6 GHz for slot dimensions of L = 3.74 mm and W = 0.4 mm. Length and width increased 11% and 19%, respectively. The results of these increase are presented in Fig. 46 and on Table VI. Fig. 47 represents the $S_{1,1}$ behaviour.

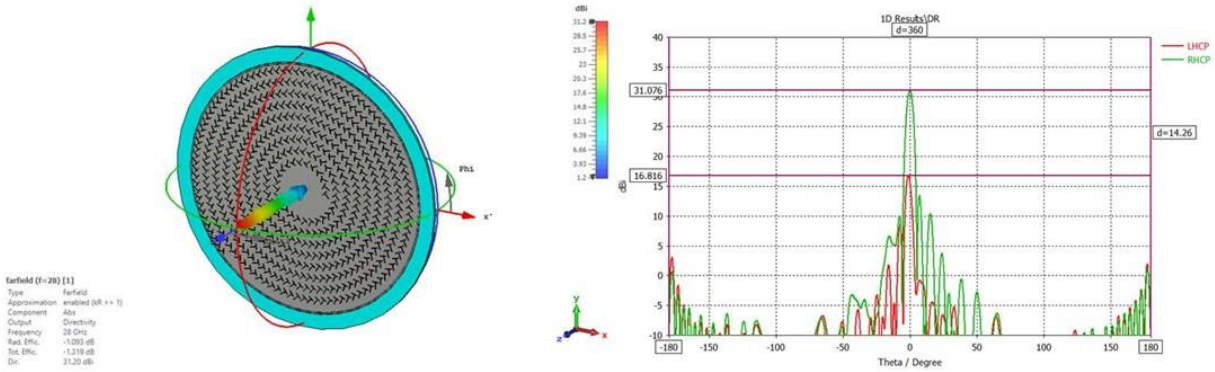

Fig. 46 – Farfield 3D Radiation Pattern and Cross Polarization Level for a completed RLSA @ 28.6 GHz for L = 3.74 mm and W = 0.4 mm.

Table VI – *CST STUDIO Suite* RLSA antenna results @ 28.6 GHz for L = 3.74 mm and W = 0.4 mm.

H [mm]	1.575
h_core [mm]	1.25
Dir. [dB]	31.2
$S_{1,1}$ [dB]	-19.0
X-POL [dB]	-14.26
SLL [dB]	-17.6
Rad. Efficiency [dB]	-1.093
Total Efficiency [dB]	-1.319

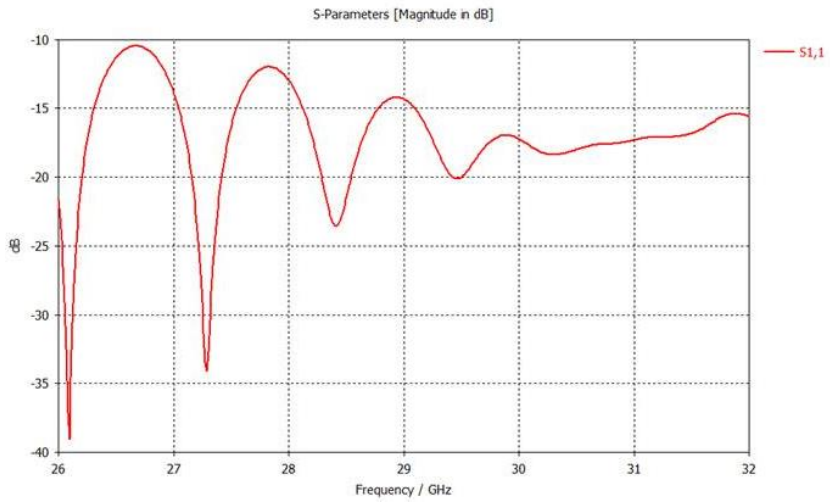

Fig. 47 – $S_{1,1}$ levels for a completed RLSA @ 28.6 GHz for L = 3.74 mm and W = 0.4 mm.

Although a good result at 28.6 GHz is obtained at this stage, the feeding process needs to be changed. A single cable might be the simplest solution but achieving the proposed solution of h_core = 1.25 mm requires a great deal of precision. A new feeding system is proposed in section 3.4 but first a beam-tilt antenna is tested in the next section.

3.3 Beam-tilt aperture design

This section aims to construct and test a RLSA antenna using the method explained in section 2.2.5. Tilt angle is set at $\alpha_0 = 25.4^o$ and W at 0.4 mm. The tilt angle α_0, is set at 25.4º to match a previously designed transmit array. Parameters a and b from equation (2.28) are set to 1.07 and 0.29, respectively. A sweep of L is made from 3.37 mm to 3.6 mm. A greater value for L is not considered because slot pair spacing does not allow. For lengths greater than 3.6mm pairs would intersect with each other.

First, we distribute the slots using the KH3Dslot script over the elongated spiral as illustrated in Fig. 48. The directivity of the arrays is shown in Table VII and later compared with the values of CST STUDIO Suite.

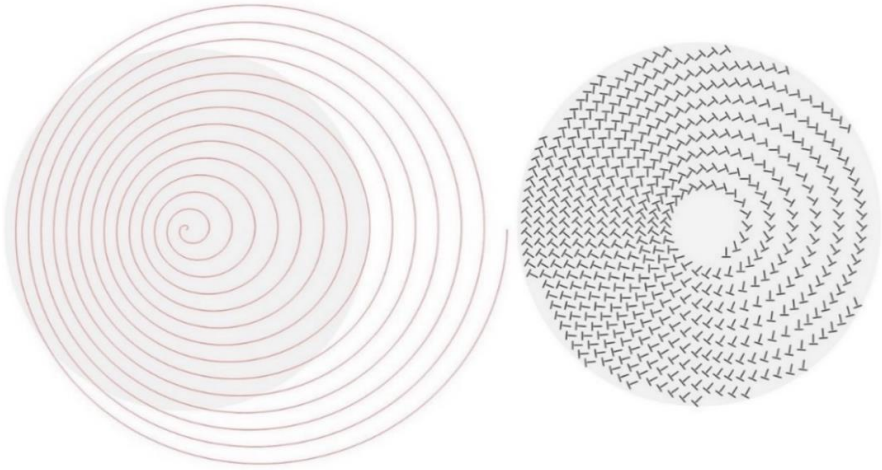

Fig. 48 – Slot Array in KH3Dslot script for a $\alpha_0 = 25.4^o$ beam tilt RLSA antenna

Table VII – KH3Dslot directivity results for a $\alpha_0 = 25.4^o$ beam tilt RLSA antenna

L [mm]	3.37	3.5	3.6
Dir. [dB]	29.95	28.98	29.0

In KH3Dslot slots are arranged to perform LHCP. The following figure, Fig. 49, presents the LHCP and RHCP electric farfields. The presented beam inclination achieved in the GO/PO method agrees with the formulation established in section 2.2.5. Although the method is successful in achieving the proposed beam inclination Table VII shows directivity values are practically equal. A full wave analysis is needed to further validate the script and obtain a realistic value for the directivity.

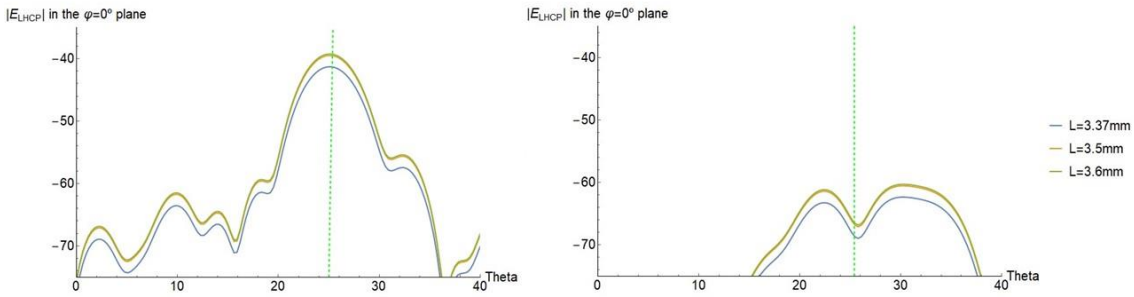

Fig. 49 – LHCP and RHCP electric farfields for $\alpha_0 = 25.4^o$ beam tilt RLSA antenna

For CST STUDIO Suite simulations, PPW height and h_core are 1.575mm and 1.25mm, respectively as before. The resulting model can be seen on Fig. 50.

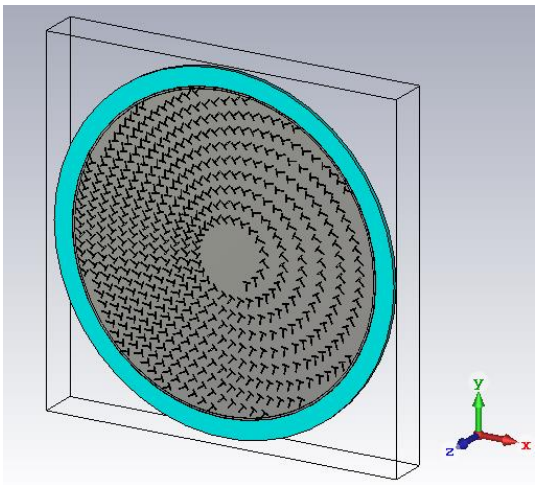

Fig. 50 – Beam Tilted RLSA model for $\alpha_0 = 25.4^o$.

Fig. 51 shows $S_{1,1}$ for three slot lengths: 3.37mm, 3.5mm and 3.6mm. By examining the graphic, good levels of $S_{1,1}$ are achieved by all tested lengths. An approximate mean level of -15 dB is accomplished for the studied frequencies. After sweeping through all the combinations in length and its corresponding results a best performance can be obtained if L = 3.6 mm at 28.6 GHz. Table VIII presents the results.

Table VIII – *CST STUDIO Suite* Beam Tilted RLSA, $\alpha_0 = 25.4^o$, L=3.6 mm, W = 0.4 mm @ 28.6 GHz

H [mm]	1.575
h_core [mm]	1.25
Dir. [dB]	28.85
$S_{1,1}$ [dB]	-19.0
X-POL [dB]	-17.4
Rad. Efficiency [dB]	-1.154
Total Efficiency [dB]	-1.207

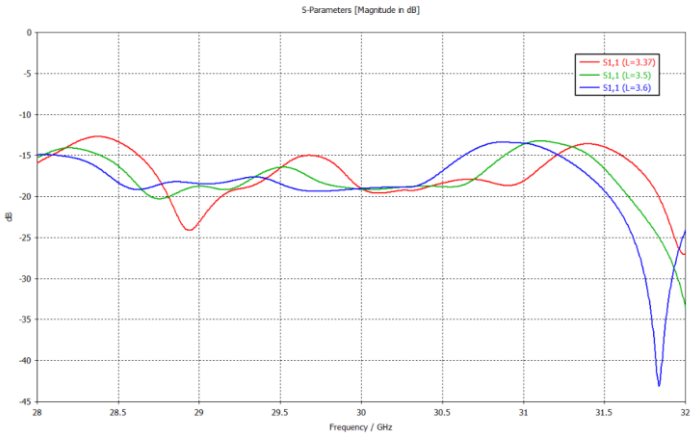

Fig. 51 – $S_{1,1}$ for Beam Tilted RLSA, $\alpha_0 = 25.4^o$ for different lengths: L=3.37 mm (red), L=3.5 mm (green) and L=3.6 mm (blue).

Fig. 52 presents a three-dimensional directivity radiation pattern for beam tilt RLSA design at 28.6 GHz. The angle of the main lobe can be observed as it is intended to be and Fig. 53 confirms $\alpha_0 =$ 25.4º and represents the X-Pol level. X-Pol levels appear to be smaller relative to RLSA slot distribution for no beam tilt, $\alpha_0 = 0º$. This reduction is consistent with previous articles describing the effects of beam inclination on internal RLSA antenna reflections.

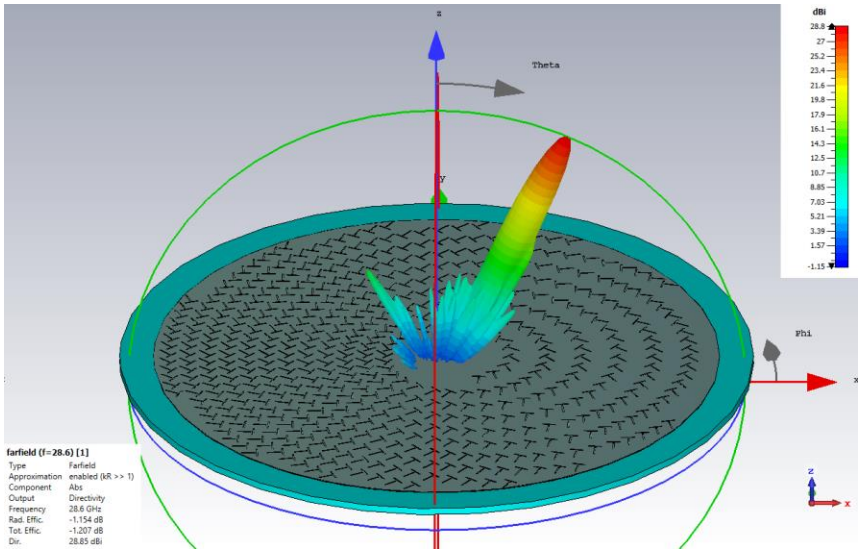

Fig. 52 – Farfield 3D Radiation Pattern for Beam Tilted RLSA, $\alpha_0 =$ 25.4º, L=3.6mm.

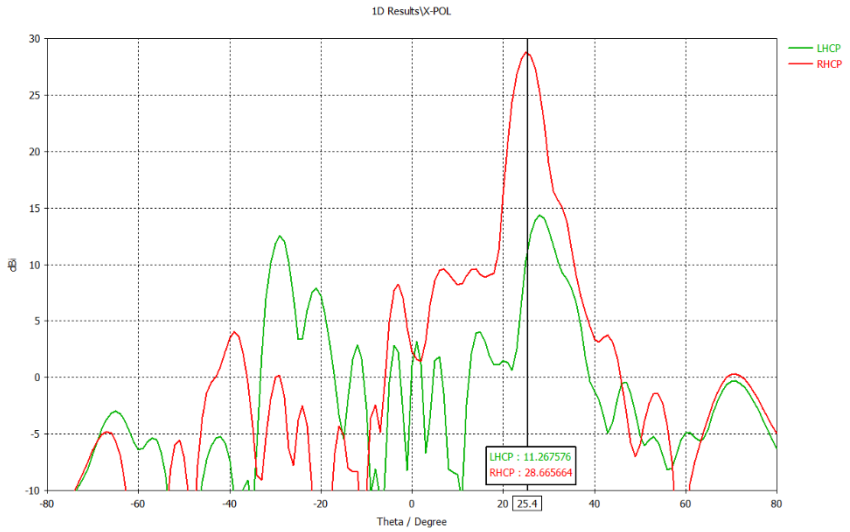

Fig. 53 – Cross Polarization Level for Beam Tilted RLSA, $\alpha_0 =$ 25.4º, L=3.6mm, W =0.4mm.

It is clear from the full-wave analysis results, the slots positions are correct to achieve $\alpha_0 =$ 25.4º beam tilt. Directivity values in KH3Dslot script are in the same order of magnitude as in *CST STUDIO Suite*. It is determined KH3Dslot can be used to predict directivity and to compute the slot pair positioning and its angles to achieve the desired beam tilt.

It was stated at the end of section 3.2 a new way of feeding the antenna is required and the same is true for the beam-tilt RLSA antenna. The next section details all the tests and simulations in the new feed design process.

3.4 New feed design

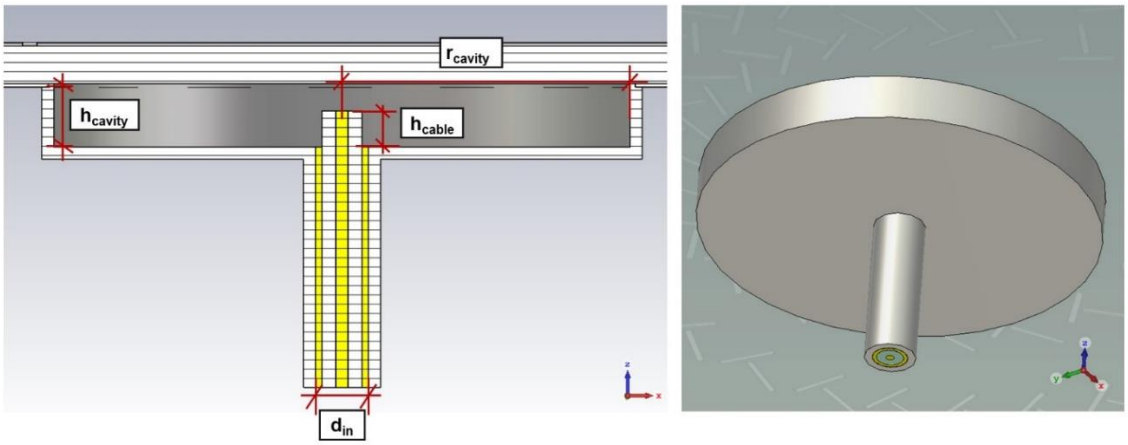

Fig. 54 – New feed for RLSA antennas

Since the design is new, for a first approach simulations run for a RLSA with no cut slots in the top plate of the PPW to fast-track results. The first step of the design is to define the parameters intervals. The cavity radius, r_{cavity}, first is tested using $\frac{\lambda_0}{4}$ increments until it reaches the point where the first pair of slots is found. The height, h_{cavity}, follows the condition (2.5) and is tested in the interval [1;5] mm with 0.5 mm steps. The height of the cable, h_{cable}, is tested according to h_{cavity}. It goes from the lowest setting to the maximum height possible. The entry hole for the cable, $d_{in,}$ depends on the cable being used. For the feed, coaxial cable EZ-86 is chosen. Specifications are detailed on Table IX.

Electric and magnetic fields of the feed can be seen in Fig. 55. The difference in magnitude is compared with the previous way of feeding the structure. A smaller amount of energy passes from the cable to the PPW once the new feed is used. This may be related to Air/Duroid 5880 interface present at the bottom of the antenna which can add extra internal reflections.

Table IX – EZ-86 Coaxial Cable specifications

	EZ-86 Measures
Core diameter [mm]	0.51
Dielectric diameter [mm]	1.676
Shielding diameter [mm]	2.2

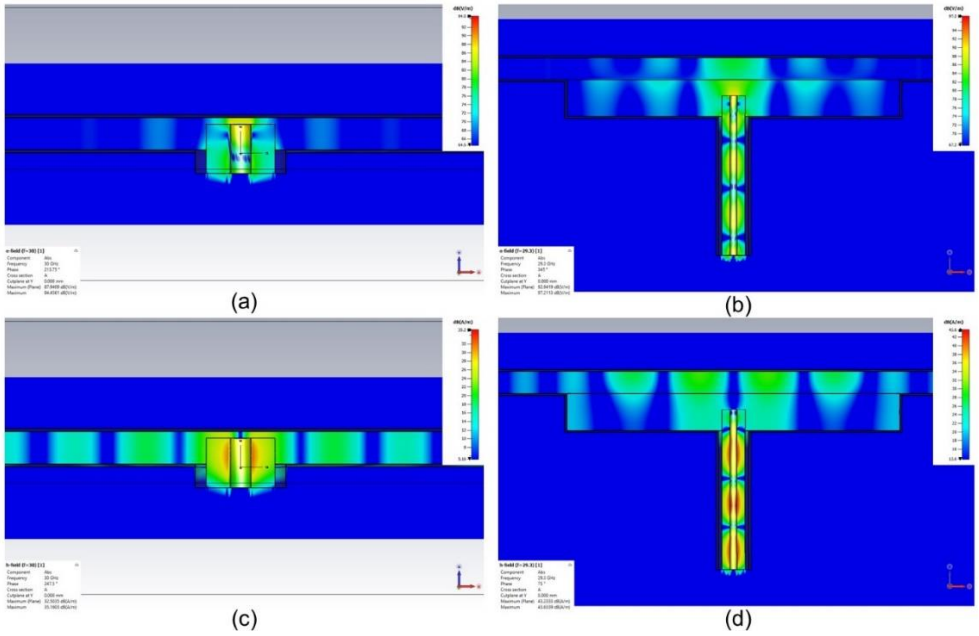

Fig. 55 – Electric and Magnetic Fields Feed comparison: coaxial cable E-field (a), cavity E-field (b), coaxial cable H-field (c) and cavity H-field (d).

After simulating multiple parameter combinations, not a great deal of solutions appear to be viable. Low levels of $S_{1,1}$ are observed throughout all the permutations. Small and narrow magnitude dips are common while performing the tests with no slots. Measures are chosen by looking at the depressions in $S_{1,1}$ and at which frequency bands they occur. Based on the previous RLSA models, a better performance is achieved from 28 to 29 GHz thus, a set of parameters is selected to fit the preferred band. Fig. 56 shows $S_{1,1}$ response for the set of feed parameters detailed in

Table X.

The solution to surpass such limitation may rely on tunning the feed structure and slots together. The already provisional parameters are tested and tweaked to achieve good performance. Final results from re-tunning efforts are presented in the next section.

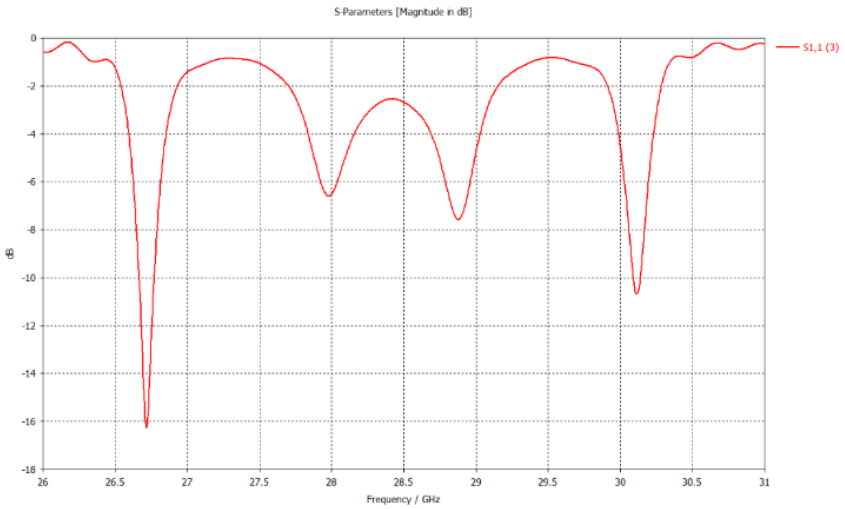

Fig. 56 – $S_{1,1}$ for r_{cavity} = 12.5 mm, h_{cavity}= 2.5 mm, h_{cable} = 1.5 mm, d_{in} = 2.2 mm

Table X – Provisional feed measures

r_{cavity} [mm]	12.5
h_{cavity} [mm]	2.5
h_{cable} [mm]	1.5
d_{in} [mm]	2.2

3.5 Final CP-RLSA models

To finalize the design process, two main modifications are made. First, the absorber rim is no longer considered as a component for both RLSA models. The absorbent thickness proposed is not viable because it is too thin and becomes difficult to assemble a prototype. The second and final change is the re-tunning of the new feeding cavity.

For the changes in the cavity, the efforts are placed on the cavity radius, r_{cavity}. A parameter sweep of is tested around the preceding value of 12.5 mm. The interval checked is [12; 13] mm. The cable remains with the same depth inside and cavity height is varied by a small amount of ± 0.1 mm. All the simulations are for the RLSA with no beam tilt, $\alpha_0 = 0º$. Once a good result is achieved, the same feed measurements are assessed for $\alpha_0 = 25.4º$ RLSA antenna. Fig. 57 represents the $S_{1,1}$ for the final designed RLSA. The two RLSA antennas have final bandwidth of approximately 800 MHz (frequency band bellow -10 dB). The results for the final feed are as shown on Table XII for both RLSA antennas described in Table XI.

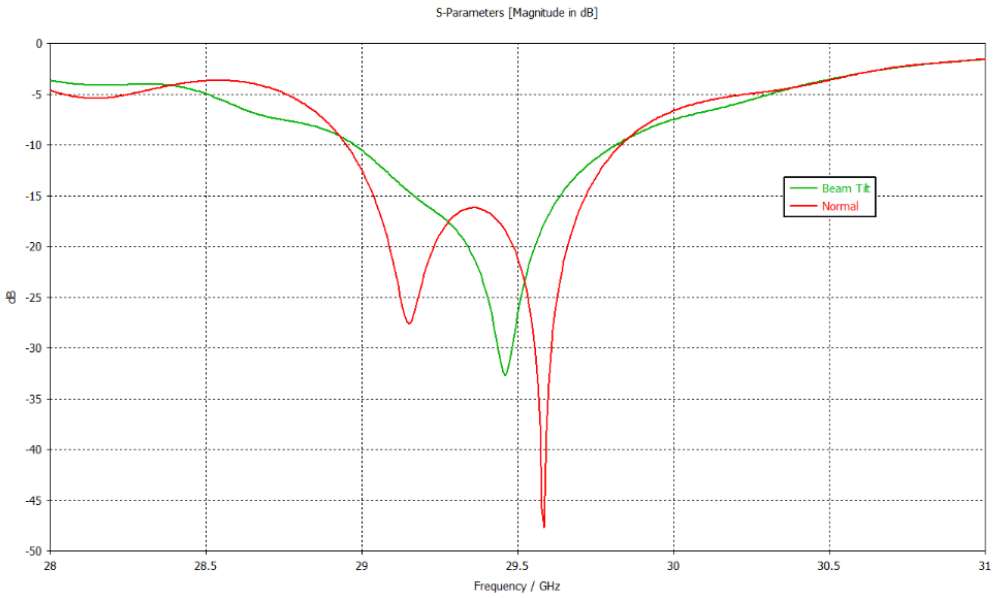

Fig. 57 – $S_{1,1}$ for both final RLSA simulated models: $\alpha_0 = 0^o$ (red) and $\alpha_0 = 25.4^o$ (green)

Table XI – PPW and Slot measures for both RLSA antennas.

	α_0	
	0^o	25.4^o
H [mm]	1.575	
L [mm]	3.74	3.60
S_φ	$0.62\lambda_g$	
W [mm]	0.40	

Table XII – Final feed measures for both RLSA antennas

	α_0	
	0^o	25.4^o
r_{cavity} [mm]	12	
h_{cavity} [mm]	2.5	
h_{cable} [mm]	1.5	
d_{in} [mm]	2.2	

The best results for both cases occur in the [29.0; 29.2] GHz band which is closer to the initial proposed frequency. Fig. 58, Fig. 59 and Fig. 60 illustrate the realized gain radiation patterns at 29.0, 29.1 and 29.2 GHz, respectively and Table XIII, Table XIV and Table XV the corresponding outcomes.

Table XIII – RLSA antenna parameter results @ 29.0 GHz

f = 29.0 GHz	α_0	
	0^o	25.4^o

Realized Gain [dB]		29.4	26.4
$S_{1,1}$ [dB]		-12.7	-10.5
X-POL [dB]		-7.9	-20.9
SLL [dB]	φ = 0º	-17.6	-10.6
	φ = 90º	-16.3	
Rad. Efficiency [dB]		-0.15	-0.13
Total Efficiency [dB]		-0.39	-0.53

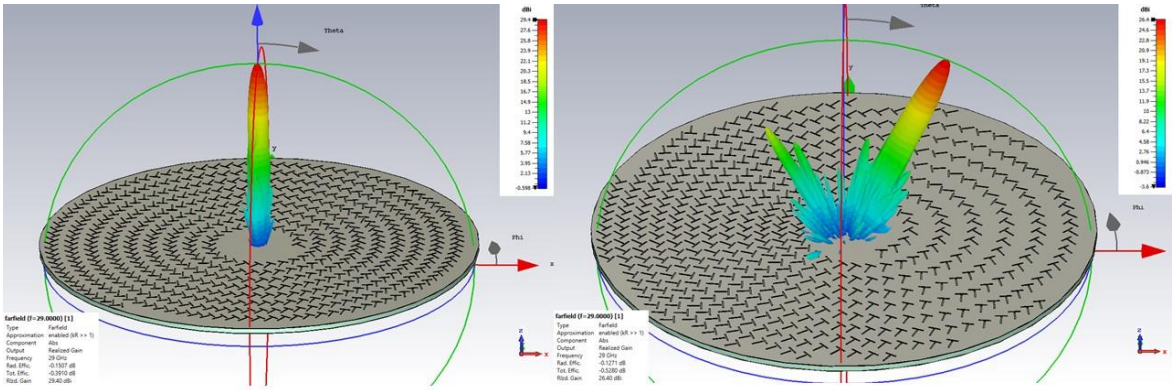

(a) (b)

Fig. 58 – Farfield Realized Gain 3D Radiation Pattern@29.0GHz: $\alpha_0 = 0º$ (a) and $\alpha_0 = 25.4º$ (b

Table XIV – RLSA antenna parameter results @ 29.1 GHz

f = 29.1 GHz		α_0	
		0º	25.4º
Realized Gain [dB]		29.33	26.45
$S_{1,1}$ [dB]		-22.0	-13.2
X-POL [dB]		-7.99	-28.0
SLL [dB]	φ = 0º	-19.4	-11.1
	φ = 90º	-16.4	
Rad. Efficiency [dB]		-0.15	-0.12
Total Efficiency [dB]		-0.18	-0.33

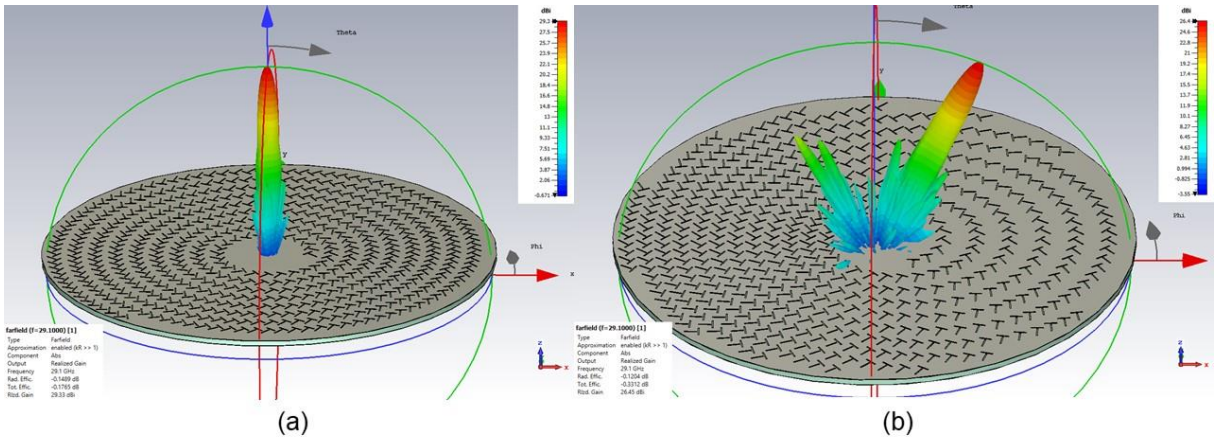

Fig. 59 – Farfield Realized Gain 3D Radiation Pattern@29.1GHz: $\alpha_0 = 0^o$ (a) and $\alpha_0 = 25.4^o$ (b).

Table XV – RLSA antenna parameter results @ 29.2 GHz

f = 29.2 GHz		α_0	
		0^o	25.4^o
Realized Gain [dB]		29.2	26.34
$S_{1,1}$ [dB]		-22.9	-15.8
X-POL [dB]		-8.08	-40.6
SLL [dB]	$\varphi = 0^o$	-17.6	-11.5
	$\varphi = 90^o$	-16.3	
Rad. Efficiency [dB]		-0.114	-0.117
Total Efficiency [dB]		0.136	-0.233

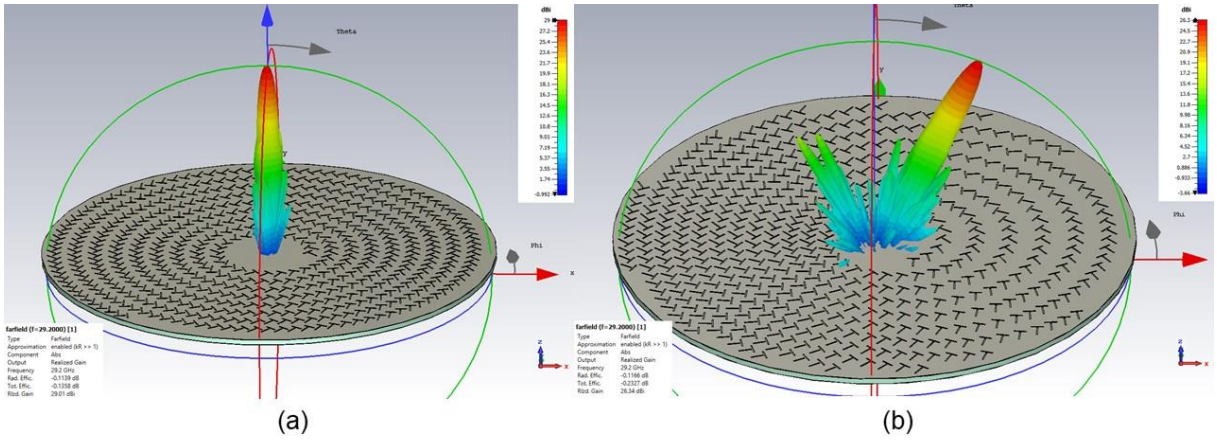

Fig. 60 – Farfield Realized Gain 3D Radiation Pattern@29.2GHz: $\alpha_0 = 0^o$ (a) and $\alpha_0 = 25.4^o$ (b).

In the previous tables none of RLSA models for $\alpha_0 = 25.4^o$ main lobes cross the plane $\varphi = 90^o$ and thus the SLL is not considered. Additionally, a sudden increase in of radiation and total efficiency is deceiving. CST STUDIO Suite considers the energy that escaped at the antenna perimeter as radiated

energy which is true but not in the main lobe. Further measurements are necessary for main lobe efficiency.

RLSA antenna with $\alpha_0 = 0º$ has 1072 slots (536 pairs) and RLSA antenna with $\alpha_0 = 25.4º$ has 998 slots (499 pairs).

3.6 Manufacture process

3.6.1 Feed Cavity

Fig. 61 – Feed cavity final constructed model

The final model is made out of brass. There are slight variations, but the main parameters remain the same: $r_{cavity} = 12$ mm and $h_{cavity} = 2.5$ mm. The walls increased in thickness to 1mm to ensure a sturdy structure and a small ledge is added on top of the cavity walls to facilitate the junction between the cavity, and the bottom plate. An extra piece is added to the bottom of the structure. A bolting nut is used to secure the coaxial cable in place and allow more precise adjustments. Fig. 61 shows the final result.

3.6.2 Printed Circuit

The manufacture of the top and bottom plate of the antennas is accomplished through a printed process. From the CAD models developed in CST STUDIO Suite, 4 masks are generated: for a normal beam, for a beam tilted beam and ground plate masks. Fig. 62 shows the three masks used to print on both sides of a ROGER 5880 substrate with 1.575mm.

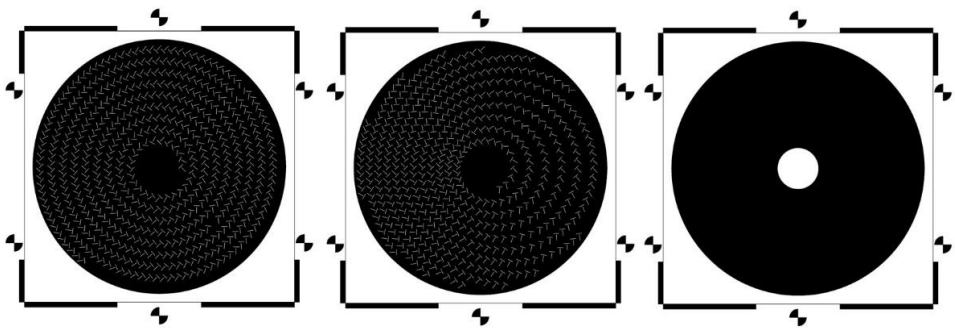

Fig. 62 – Masks used for the production of the printed circuit

3.6.3 Antenna support

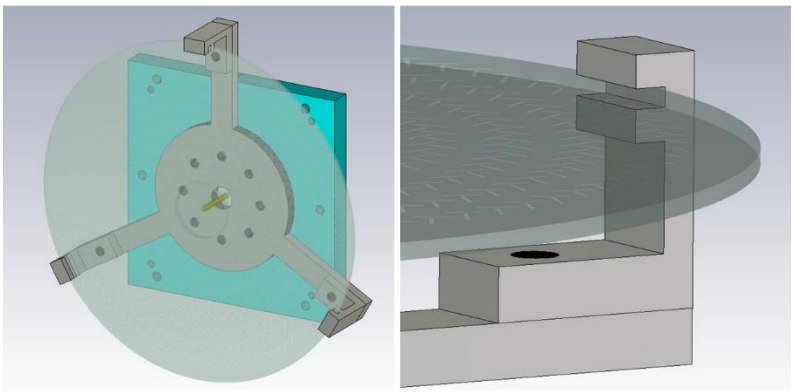

Fig. 63 – CAD antenna support model

To hold the antenna in place a support structure is devised. Fig. 63 represents the CAD model conceived. The support is adapted for a previously constructed platform, represented in the Fig. 63 in blue. It is comprised of a central ring with 8 holes to fit screws and 3 arms separated by 120º. At the end of each arm there is a claw which holds the RLSA antenna. Each claw is screwed to the respective arm.

Chapter 4

Conclusions

4.1 Main achievements

The two antennas in this work are developed for user satellite access in the ka band, more precisely from 29.0 to 29.2 GHz. The first RLSA antenna radiates parallel to the normal direction, $\alpha_0 = 0^o$, and the second RLSA antenna radiates at an angle of $\alpha_0 = 25.4^o$ relative to the normal direction. They both have a 150mm diameter and are fed by a new designed cavity and a coaxial cable placed under the structure.

The study consists of a detailed examination of all the components on the RLSA antenna and their influence during the design process. The first component is the circular PPW. Distance between plates and radius are studied to match the circular PPW and the coaxial cable feed to minimize internal reflections. An option of placing an absorber rim and its thickness at the perimeter are also studied to assure reflected fields do not influence the results. The second component is the dielectric substrate to insert between the parallel plates. Three materials are tested: air, Duroid 5880 and FR-4. The difference in wave propagation and internal reflections is studied. The third component are the slot pairs. A reduced model equivalent to a quarter of a RLSA antenna is proposed and tested for a single slot pair. Lengths and radial position of the pair are varied to observe slot field behaviour. The final step is to join all the previous parts and test. Slot positioning and angles are achieved through the developed GO/PO framework, KH3Dslot, and by CST STUDIO Suite macros. A preliminary analysis is carried out to choose the best material. Electric permittivity of the substrates directly affects the guided wavelength. This variation influences the slot dimensions and their spacing which allows for a denser slot distribution and consequently, a higher aperture efficiency. On the other hand, a surge in internal reflections is observed with the increase of electric permittivity. The compromises are analysed first by testing a partially slot covered top plate is tested and then a fully slot covered antenna. Duroid 5880 substrate is chosen for the increase in directivity and the small surge in $S_{1,1}$ parameter. Slot dimensions and spacings are adjusted to improve the performance. The same process is conducted for the beam tilted RLSA. For this case slot positioning and angles are obtained through the same GO/PO framework and and CST STUDIO Suite macro. A fully covered beam tilted RLSA is simulated and tested. Slot dimensions are increased to improve antenna gain. To feed the antennas a new cavity is designed and attached to the PPW bottom plate. This solution came out of need for a better control in coaxial cable insertion in the RLSA. Multiple heights and diameters for the cavity are tested in conjunction with the slot covered top plate. The same cavity dimensions for a RLSA antenna with $\alpha_0 = 0^o$ work also well for RLSA antenna with $\alpha_0 = 25.4^o$. To verify the computer models, prototypes are constructed and analysed.

The two RLSA antennas work best in the 29.0 to 29.2 GHz band. The first one averages a 29.3dB gain and the second a 26.4dB. They both present a good SLL when considering the main lobe direction.

By examining $S_{1,1}$, their bandwidth is roughly 800MHz. X-Pol levels obtained are not ideal for the first RLSA and good for the second RLSA.

In the end, two small 150mm diameter antennas and newly designed feeding process working in the k_a band are accomplished. The RLSA antenna with $\alpha_0 = 0º$ has 1072 slots (536 pairs) and RLSA antenna with $\alpha_0 = 25.4º$ has 998 slots (499 pairs). Experimental result will be obtained soon to validate both RLSA designs.

4.2 Future Work

Some subjects in this work need further attention. To improve on the X-Pol, gain and efficiency levels of the RLSA antenna with $\alpha_0 = 0º$, two options can be added. An absorbent slim enough can be fabricated to place at the edge of the PPW. Additionally, as proposed in [12], a matching spiral is a possibility previously explored in literature used to radiate the remaining power at the perimeter of the antenna. Moreover, X-Pol, gain and efficiency improvement through slot coupling control is the next step to upgrade the designed RLSA antennas. Examples can be found in [50] or [34]. By varying the slot length along the radial distance, a better distribution of the fields and phase can be achieved. Furthermore, by doing so a better beam shape with less side lobes can be attained. Finally, the slot positioning for a beam tilted RLSA described in section 2.2.5 can be improved upon. References [15] and [45] present a more precise formulation for a beam tilt CP-RLSA.

Some possible topics related to this dissertation originate new thesis. The slot coupling control is an interesting topic to develop computationally and to build on top of the KH3Dslot script. There is literature on the subject, and it can be used to improve the two designed RLSA antennas. Another matter which can be valuable is a dual-band CP-RLSA. Since slot length when tunning the working frequency, a slot length difference inside the same pair can lead to a dual working frequency. Moreover, a double spiral RLSA [35] can be tested in which the two spirals are tuned to different frequencies. The big challenge of a dual-band CP-RLSA [43] is making sure the first set of slots does not disturb the propagating fields meant for the second set of slots, and vice-versa.

References

[1] "LEO, GEO, MEO Satellites – What's The Difference? - Simple Flying." https://simpleflying.com/leo-geo-meo-satellites-whats-the-difference/ (accessed Feb. 01, 2021).

[2] "Starlink." https://www.starlink.com/ (accessed Feb. 01, 2021).

[3] "Starlink - Satellite Missions - eoPortal Directory." https://directory.eoportal.org/web/eoportal/satellite-missions/s/starlink (accessed Feb. 01, 2021).

[4] "SpaceX surpasses 1,000-satellite mark in latest Starlink launch - SpaceNews." https://spacenews.com/spacex-surpasses-1000-satellite-mark-in-latest-starlink-launch/ (accessed Feb. 01, 2021).

[5] K. K., "Recent annular slot array experiments," *1958 IRE Int. Conv. Rec.*, vol. 19, no. 604, [Online]. Available: https://ieeexplore.ieee.org/stamp/stamp.jsp?tp=&arnumber=1150575.

[6] F. Goebels and K. Kelly, "Arbitrarily polarized planar antennas," Mar. 2005, pp. 119–127, doi: 10.1109/irecon.1959.1150781.

[7] M. Ando, K. Sakurai, and N. Goto, "A Radial Line Slot Antenna for 12 GHz Band Satellite TV Reception," *IEEE Trans. Antennas Propag.*, vol. 34, no. 10, pp. 1269–1272, 1986, doi: 10.1109/TAP.1986.1143744.

[8] M. Ando, K. Sakurai, and N. Goto, "Characteristics of a Radial Line Slot Antenna for 12 GHz Band Satellite TV Reception," *IEEE Trans. Antennas Propag.*, vol. 34, no. 10, pp. 1269–1272, 1986, doi: 10.1109/TAP.1986.1143744.

[9] M. Ando, J. Takada, T. Numata, and N. Goto, "A Linearly-Polarized Radial Line Slot Antenna," in *1988 IEEE AP-S. International Symposium, Antennas and Propagation*, pp. 836–839, doi: 10.1109/APS.1988.94209.

[10] M. Ando, T. Numata, J. I. Takada, and N. Goto, "A Linearly Polarized Radial Line Slot Antenna," *IEEE Trans. Antennas Propag.*, vol. 36, no. 12, pp. 1675–1680, 1988, doi: 10.1109/8.14389.

[11] J. ichi Takada, M. Ando, and N. Goto, "A Reflection Cancelling Slot Set in a Linearly Polarized Radial Line Slot Antenna," *IEEE Trans. Antennas Propag.*, vol. 40, no. 4, pp. 433–438, 1992, doi: 10.1109/8.138845.

[12] M. Ando, M. Takahashi, M. Natori, J. Takada, and N. Goto, "Single-layered radial line slot antenna for DBS reception," in *Conference Proceedings - European Microwave Conference*, 1990, vol. 2, no. 20, pp. 1541–1546, doi: 10.1109/euma.1990.336287.

[13] M. Ando, M. Takahashi, J. Takada, and N. Goto, "A slot design for uniform aperture field distribution in single-layered radial line slot antennas," in *IEEE Antennas and Propagation Society, AP-S International Symposium (Digest)*, 1991, vol. 2, pp. 930–933, doi: 10.1109/aps.1990.115261.

[14] S. A. Schelkunoff, "Some Equivalence Theorems of Electromagnetics and Their Application to Radiation Problems," *Bell Syst. Tech. J.*, vol. 15, no. 1, pp. 92–112, 1936, doi: 10.1002/j.1538-7305.1936.tb00720.x.

[15] J. Hirokawa, M. Ando, and N. Goto, "Analysis of slot coupling in a radial line slot antenna for DBS reception," *IEE Proc. H Microwaves, Antennas Propag.*, vol. 137, no. 5, pp. 249–254, 1990, doi: 10.1049/ip-h-2.1990.0049.

[16] M. Takahashi, J. Takada, M. Ando, and N. Goto, "High Efficiency Flat Array Antennas for DBS Reception," in *1991 21st European Microwave Conference*, 1991, vol. 1, pp. 629–634, doi: 10.1109/EUMA.1991.336372.

[17] M. Takahashi, J. Takada, M. Ando, and N. Goto, "Characteristics of small-aperture, single-layered, radial-line slot antennas," *IEE Proc. H Microwaves, Antennas Propag.*, vol. 139, no. 1, pp. 79–83, 1992, doi: 10.1049/ip-h-2.1992.0013.

[18] K. I. Member, J. -I Takada, M. Ando, and N. Goto, "A radial line slot antenna without a slow wave structure," *Electron. Commun. Japan (Part I Commun.*, vol. 76, no. 7, pp. 81–88, 1993, doi: 10.1002/ecja.4410760709.

[19] M. Takahashi, M. Yoshiie, and M. Abe, "Basic design of beam tilting radial line slot antennas," *IEEE Antennas Propag. Soc. AP-S Int. Symp.*, vol. 3, pp. 1384–1387, 1995, doi: 10.1109/aps.1995.530833.

[20] P. W. Davis, "Experimental investigations into a linearly polarized radial slot antenna for DBS TV in Australia," *IEEE Trans. Antennas Propag.*, vol. 45, no. 7, pp. 1123–1129, 1997, doi: 10.1109/8.596903.

[21] P. W. Davis and M. E. Bialkowski, “Comparing beam squinting and reflection cancelling slot methods for return loss improvement in RLSA antennas,” in *IEEE Antennas and Propagation Society, AP-S International Symposium (Digest)*, 1997, vol. 3, pp. 1938–1941, doi: 10.1109/aps.1997.631715.

[22] P. W. Davis and M. E. Bialkowski, “Linearly polarized radial-line slot-array antennas with improved return-loss performance,” *IEEE Antennas Propag. Mag.*, vol. 41, no. 1, pp. 52–61, 1999, doi: 10.1109/74.755027.

[23] M. E. Bialkowski and P. W. Davis, “Predicting the radiation pattern of a radial line slot array antenna,” *Asia-Pacific Microw. Conf. Proceedings, APMC*, vol. 1, pp. 162–165, 1999, doi: 10.1109/apmc.1999.828075.

[24] M. E. Bialkowski and P. W. Davis, “Unified design of a single-layer radial line slot array antenna,” *2000 30th Eur. Microw. Conf. EuMC 2000*, pp. 2–5, 2000, doi: 10.1109/EUMA.2000.338865.

[25] M. Sierra Castañer, M. Sierra Pérez, M. Vera Isasa, and J. L. Fernández Jambrina, “Design method, analysis and prototypes of radial line slot antennas,” *IEEE Antennas Propag. Soc. AP-S Int. Symp.*, vol. 3, pp. 574–577, 2001, doi: 10.1109/APS.2001.960162.

[26] M. VERA-ISASA, M. SIERRA-CASTAÑER, and M. SIERRA-PÉREZ, “Design of Circular Polarized Radial Line Slot Antennas,” *Int. J. Wirel. Opt. Commun.*, vol. 01, no. 02, pp. 179–189, 2003, doi: 10.1142/s0219799503000161.

[27] M. Vera-Isasa, M. Sierra-Castañer, and M. Sierra-Pérez, “Slot antenna with a tilted beam for satellite reception,” *Microw. Opt. Technol. Lett.*, vol. 36, no. 5, pp. 392–394, 2003, doi: 10.1002/mop.10773.

[28] K. Sudo, J. Hirokawa, M. Ando, and M. Sierra-Casta??er, “Full-model analysis of a radial line slot antenna including the feeder and improvement of aperture field uniformity by shift of position of each slot pair in the radial direction,” in *IEEE Antennas and Propagation Society, AP-S International Symposium (Digest)*, 2004, vol. 3, pp. 2349–2352, doi: 10.1109/aps.2004.1331843.

[29] J. I. Herranz-Herruzo, A. Valero-Nogueira, and M. Ferrando-Bataller, “Optimization technique for linearly polarized radial-line slot-array antennas using the multiple sweep method of moments,” *IEEE Trans. Antennas Propag.*, vol. 52, no. 4, pp. 1015–1023, Apr. 2004, doi: 10.1109/TAP.2004.825182.

[30] M. Sierra-Castañer, M. Sierra-Pérez, M. Vera-Isasa, and J. L. Fernández-Jambrina, “Fast analysis model for radial-line slot antennas,” *Microw. Opt. Technol. Lett.*, vol. 44, no. 1, pp. 17–21, Jan. 2005, doi: 10.1002/mop.20534.

[31] M. Sierra-Castañer, M. Sierra-Pérez, M. Vera-Isasa, and J. L. Fernández-Jambrina, “Multiprobe RLSA design for DBS reception,” *Microw. Opt. Technol. Lett.*, vol. 36, no. 1, pp. 70–72, 2003, doi: 10.1002/mop.10675.

[32] M. Sierra-Castañer, M. Sierra-Pérez, and M. Vera-Isasa, “Low-cost monopulse radial line slot antenna,” *IEEE Trans. Antennas Propag.*, vol. 51, no. 2, pp. 256–263, 2003, doi: 10.1109/TAP.2003.809098.

[33] M. Albani, G. La Cono, R. Gardelli, and A. Freni, “An efficient full-wave method of moments analysis for RLSA antennas,” *IEEE Trans. Antennas Propag.*, vol. 54, no. 8, pp. 2326–2336, Aug. 2006, doi: 10.1109/TAP.2006.879197.

[34] M. Albani, A. Mazzinghi, and A. Freni, “Automatic design of CP-RLSA antennas,” *IEEE Trans. Antennas Propag.*, vol. 60, no. 12, pp. 5538–5547, 2012, doi: 10.1109/TAP.2012.2214014.

[35] A. Mazzinghi, M. Albani, and A. Freni, “Double-spiral linearly polarized RLSA,” *IEEE Trans. Antennas Propag.*, vol. 62, no. 9, pp. 4900–4903, 2014, doi: 10.1109/TAP.2014.2336691.

[36] T. Nguyen, S. Member, J. Hirokawa, M. Ando, and M. Sierra Casta, “Design of mm-Wave RLSAs with Lossy Waveguides by Slot Coupling Control Techniques,” no. 9, 2015, doi: 10.1587/transcom.E98.B.1865.

[37] T. Purnamirza, D. Kristanto, and I. M. Bin Ibrahim, “A design of compact radial line slot array (RLSA) antennas for Wi-Fi market needs,” *Prog. Electromagn. Res. Lett.*, vol. 64, no. September 2018, pp. 21–28, 2016, doi: 10.2528/PIERL16083101.

[38] T. Purnamirza, I. M. Ibrahim, P. Prowadi, and F. Amillia, “Small radial line slot array (RLSA) antennas for Wi-Fi 5.8 GHz devices,” *International Journal on Communications Antenna and Propagation*, vol. 7, no. 5. Praise Worthy Prize S.r.l, pp. 397–402, 2017, doi: 10.15866/irecap.v7i5.10431.

[39] T. Purnamirza, P. Budikesuma, I. M. Bin Ibrahim, D. Rahmi, and R. Susanti, “A small RLSA antenna utilizing the specification of Back Fires 17 dBi LAN Antennas,” *Telkomnika (Telecommunication Comput. Electron. Control.*, vol. 16, no. 6, pp. 2871–2878, Dec. 2018, doi:

10.12928/TELKOMNIKA.v16i6.10414.
[40] T. Purnamirza, S. Hasbi, I. M. Bin Ibrahim, Mulyono, F. Amillia, and D. Rahmi, “A radial line slot array (RLSA) antenna with the specifications of 16 dBi outdoor patch antenna,” *Telkomnika (Telecommunication Comput. Electron. Control.*, vol. 16, no. 1, pp. 46–52, 2018, doi: 10.12928/TELKOMNIKA.v16i1.6727.
[41] M. R. U. Islam and T. A. Rahman, “Novel and simple design of multi layer Radial Line Slot Array (RLSA) antenna using FR-4 Substrate,” in *2008 Asia-Pacific Symposium on Electromagnetic Compatibility and 19th International Zurich Symposium on Electromagnetic Compatibility, APEMC 2008*, 2008, pp. 843–846, doi: 10.1109/APEMC.2008.4560007.
[42] T. Purnamirza, T. A. Rahman, and M. H. Jamaluddin, “The extreme beamsquint technique to minimize the reflection coefficient of very small aperture radial line slot array antennas,” *J. Electromagn. Waves Appl.*, vol. 26, no. 17–18, pp. 2267–2276, Dec. 2012, doi: 10.1080/09205071.2012.733491.
[43] J. Shao, F. Yang, R. Wang, Z. Xing, and J. Yang, “A dual band and dual circular polarization radial line slot antenna,” in *2019 IEEE International Symposium on Antennas and Propagation and USNC-URSI Radio Science Meeting, APSURSI 2019 - Proceedings*, Jul. 2019, pp. 1429–1430, doi: 10.1109/APUSNCURSINRSM.2019.8888488.
[44] M. J. Lopez-Morales, F. R. Varela, D. V. Vazquez, and M. S. Castaner, “Efficient Design of Radial Line Slot Antennas Using Currents Synthesis and Optimization,” *IEEE Antennas Wirel. Propag. Lett.*, vol. 19, no. 3, pp. 487–491, 2020, doi: 10.1109/LAWP.2020.2966124.
[45] M. N. Y. Koli, M. U. Afzal, K. P. Esselle, and R. M. Hashmi, “An All-Metal High-Gain Radial-Line Slot-Array Antenna for Low-Cost Satellite Communication Systems,” *IEEE Access*, vol. 8, pp. 139422–139432, Jul. 2020, doi: 10.1109/access.2020.3012787.
[46] Carlos A. Fernandes, “Tool for PO analysis of RSLA antennas,” 2020.
[47] Constantine A. Balanis, *Advanced Engineering Electromagnetics*, 2nd Ed. John Wiley & Sons, 2012.
[48] C. A. Balanis, *Antenna Theory - Analysis and Design*, 4th Ed. John Wiley & Sons, 2016.
[49] “Circular polarization - Wikipedia.” https://en.wikipedia.org/wiki/Circular_polarization (accessed Dec. 12, 2020).
[50] H. Sasazawa, Y. Oshima, K. Sakurai, M. Ando, and N. Goto, “Slot Coupling in a Radial Line Slot Antenna for 12-GHz Band Satellite TV Reception,” *IEEE Trans. Antennas Propag.*, vol. 36, no. 9, pp. 1221–1226, 1988, doi: 10.1109/8.8599.
[51] J. I. Herranz, V. N. Alejandro, E. Alfonso, and V. M. Rodrigo, “Optimized design of beam-tilted linearly-polarized radial-line slot-array antennas,” in *2010 IEEE International Symposium on Antennas and Propagation and CNC-USNC/URSI Radio Science Meeting - Leading the Wave, AP-S/URSI 2010*, 2010, doi: 10.1109/APS.2010.5561023.